ISSN/0393-3016

S. PARRACINO
Department of Industrial Engineering
University of Rome "Tor Vergata", Rome, Italy
ENEA guest

S. SANTORO
Department of Earth and Sea Sciences
University of Palermo, Palermo, Italy
ENEA guest

G. MAIO
ARES Consortium, Rome, Italy
ENEA guest

M. NUVOLI
Nuclear Fusion and Safety Technologies Department
ENEA, Frascati, Italy

A. AIUPPA
Department of Earth and Sea Sciences
University of Palermo, Palermo, Italy

L. FIORANI
Nuclear Fusion and Safety Technologies Department
ENEA, Frascati, Italy

LIDAR CAMPAIGN AT STROMBOLI VOLCANO: METHODOLOGY AND RESULTS

RT/2016/31/ENEA

ITALIAN NATIONAL AGENCY FOR NEW TECHNOLOGIES,
ENERGY AND SUSTAINABLE ECONOMIC DEVELOPMENT

S. PARRACINO
Department of Industrial Engineering
University of Rome "Tor Vergata", Rome, Italy
ENEA guest

M. NUVOLI
Nuclear Fusion and Safety Technologies Department
ENEA, Frascati, Italy

S. SANTORO
Department of Earth and Sea Sciences
University of Palermo, Palermo, Italy
ENEA guest

A. AIUPPA
Department of Earth and Sea Sciences
University of Palermo, Palermo, Italy

G. MAIO
ARES Consortium, Rome, Italy
ENEA guest

L. FIORANI
Nuclear Fusion and Safety Technologies Department
ENEA, Frascati, Italy

LIDAR CAMPAIGN AT STROMBOLI VOLCANO: METHODOLOGY AND RESULTS

RT/2016/31/ENEA

ITALIAN NATIONAL AGENCY FOR NEW TECHNOLOGIES,
ENERGY AND SUSTAINABLE ECONOMIC DEVELOPMENT

LIDAR CAMPAIGN AT STROMBOLI VOLCANO: METHODOLOGY AND RESULTS

S. Parracino, S. Santoro, G. Maio, M. Nuvoli, A. Aiuppa, L. Fiorani

Riassunto

Grazie al nuovo sistema di telerilevamento ambientale BILLI – Bridge Volcanic LIDAR, messo a punto dal gruppo di ricerca FSN-TECFIS-DIM dell'ENEA (CR Frascati), è stato possibile condurre una campagna sperimentale presso l'isola di Stromboli (ME) – 24-29/06/2015, allo scopo di rilevare la CO_2 presente in eccesso all'interno del plume vulcanico, per fornire un'allerta precoce in caso di eruzione.
Tale ricerca rientra nel progetto BRIDGE - Bridging the gap between gas emissions and geophysical observations at active volcanoes (progetto patrocinato dall'European Research Council).

Parole chiave: Rischio vulcanico, Rivelazione di gas, Telerilevamento laser, Lidar ad assorbimento differenziale

Abstract

Thanks to the innovative, laser-based, remote sensing system, named BILLI – Bridge Volcanic LIDAR, developed at ENEA (RC of Frascati) by FSN-TECFIS-DIM research group, it has been possible to carry out an experimental campaign at the volcanic island of Stromboli (ME), between the 24 and the 29 of June, 2015. The main goal was to detect the exceedance of in-plume CO_2 concentration for early warning of eruptions.
The research is funded by the ERC project BRIDGE – Bridging the gap between gas emissions and geophysical observations at active volcanoes.

Keywords: *Volcanic hazard, Gas detection, Laser remote sensing, Differential absorption lidar*

INDEX

1. Introduction

The prediction of future volcanic eruptions and prompt alert of neighbouring populations could soon be a reality thanks to an entirely made-in-Italy technology recently developed by ENEA researchers of FSN-TECFIS-DIM research group.
In fact, during the experimental campaign of Stromboli volcano (Eolian Islands, Italy), carried out between the 24 and the 29 of June, 2015, the new laser radar named BILLI – BrIdge voLcanic LIdar, developed by ENEA, has been used to detect and analyze volcanic plumes.
This system, based on a very sophisticated technology, has worked twenty-four hours a day, producing 3D pictures of volcanic plumes evolution at over 3 Km (from the position of BILLI) and achieving fast and remote measurements of carbon dioxide contained in volcanic fumes. According to recent studies in volcanology, the exceedance of this chemical compound is a significant indicator/clue for early warning of eruptions [1,2,3].
For the first time, this complex system has allowed real-time distance measurements of the exceedance of in-plume CO_2 concentration, an operation otherwise rare, slow, dangerous and complex, also for the difficulties posed by distance. Thanks to its mirror system the laser beam can be oriented in any direction, aiming with the maximum accuracy at the volcanic smoke plume area to be investigated.
The first field tests were successfully performed from 13 to 17 October 2014 at Pozzuoli Solfatara in Contrada Pisciarelli (Campi Flegrei crater area, Naples, Italy) [1,2,3] with the support of researchers from the ENEA Portici Laboratory of Environmental Chemistry. Lidar retrievals were in good agreement with conventional techniques, yet based on completely independent and significantly different approaches. In that specific case, measurements were performed over short distances from the position of the system; instead, during the field campaign of Stromboli, measurements were performed over long distances without any risks for authorized personnel.
ENEA has developed this particular laser radar or lidar system, under the European Research Council's BRIDGE (Bridging the gap between gas emissions and geophysical observations at active Volcanoes) project, coordinated by Prof. Alessandro Aiuppa (University of Palermo), to provide more accurate eruption prediction models so that populations might be promptly alerted in case of danger.
It is well known that measuring carbon dioxide in volcanic smoke plumes is a scientific and technological challenge extremely important. As already mentioned, actually eruptions are proved to be preceded by a higher release of gas in the smoke plumes from the crater, such as carbon dioxide, the most reliable precursor gas of volcanic eruptions.
Measurements like these ones have never been realized until now and the laser radar has allowed to carry out scans with speed and continuity more higher than conventional in-situ instruments.
For these reasons, it would also be desirable and useful, in the near future, the installation of fixed lidar stations for volcanoes real-time monitoring.
BILLI laser radar technology can also find application in hostile environments, such as areas where a fire did break out or in industrial or urban areas subject to emissions from combustion processes.

2. Material and methods

In this section is provided an overview about BILLI system mode of operation and the application of a newly designed DIAL method for the measurement of CO_2 in volcanic plumes, for early warning of eruptions. This mathematical technique has been implemented in Matlab scripts for real-time data processing and graphic presentation of the exceedance in-plume CO_2 concentration.

2.1 The BILLI system

BILLI is a complex differential absorption lidar (DIAL) system (optical radar) for environmental remote sensing that provides ground based and range resolved remote measurements. The system is composed of a transmitter and receiver equipment. For more details, a sketch of the technical scheme and the mechanical frame are reported in Figure 1.

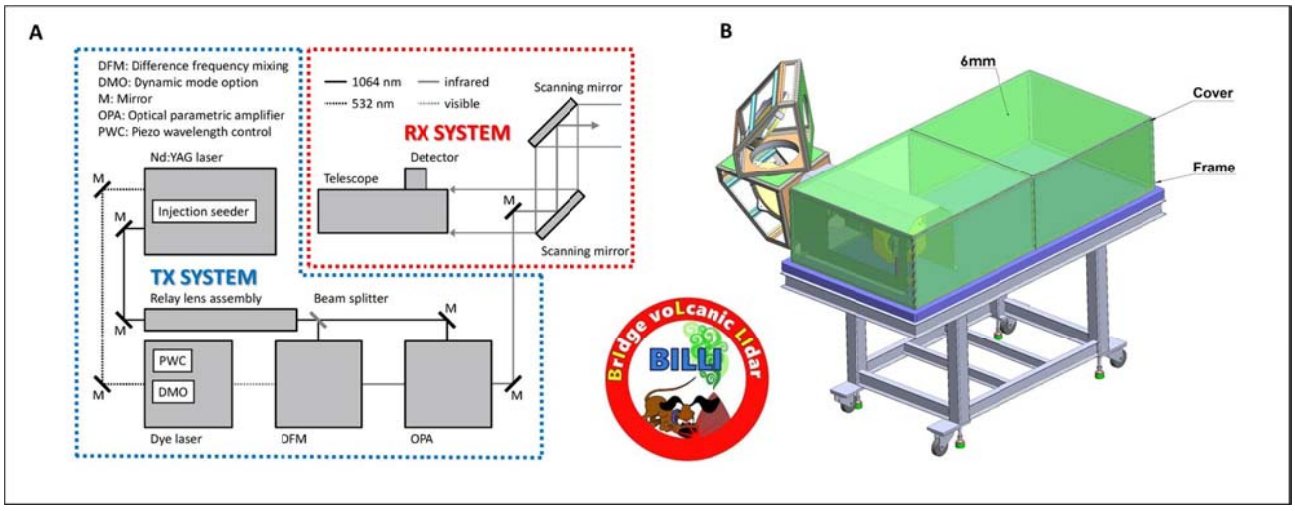

Figure 1) A - *Technical scheme of BILLI system.* **B -** *Mechanical frame of the lidar system (on the left two steering mirror to aim it to the target).*

The transmission sub-system is based on: a double grating dye-laser optically pumped by an injection seeded Nd:YAG laser (powerful, tunable and narrow-linewidth), a device for the frequency duplication (DFM – Difference Frequency Mixing) and an Optical Parametric Amplifier operating in NIR band (OPANIR); with regard to this apparatus see Figure 2.
TmHo:YLF and fiber lasers have been discarded mainly for their limited tunability (few tenths of nm) that can prevent to choose the best absorption line [4]. OPO (optical parametric amplifier) could also be a good choice, but our experience shows that they tend to be quite delicate and not easy to deploy in the harsh environment near degassing craters.
Instead, the receiver sub-system is based on: a telescope, a detector and an analogical to digital converter (ADC). The specifications of the whole system are reported in Table 1 [1,2,3].

TRANSMITTER *Pump: Quanta-Ray® Nd:YAG Laser* *Laser: Sirah PrecisionScan Dye Laser*	**Pulse energy**	25 mJ
	Pulse duration	8 ns
	Repetition rate	10 Hz
	Transmitted wavelength	2.01 μm
	Linewidth	0.04 cm^{-1}
	Beam divergence	0.5 mrad (full angle)
RECEIVER *Telescope*	**Mirror coating**	Al
	Diameter	310 mm
	Focal length	900 mm
DETECTOR *Hamamatsu InGaAs PIN Photodiode G12182*	**Diameter**	1 mm
	Photosensitivity	1.2 A W^{-1}
	Bandwidth	0 ÷ 10 MHz
	Specific detectivity	3.5×10^{11} cm $Hz^{1/2}$ W^{-1}
ADC *Agilent InfiniiVision 3000 X-Series Oscilloscopes*	**Dynamic range**	14 bit
	Sampling rate	100 Ms s^{-1}

Table 1) *BILLI specifications.*

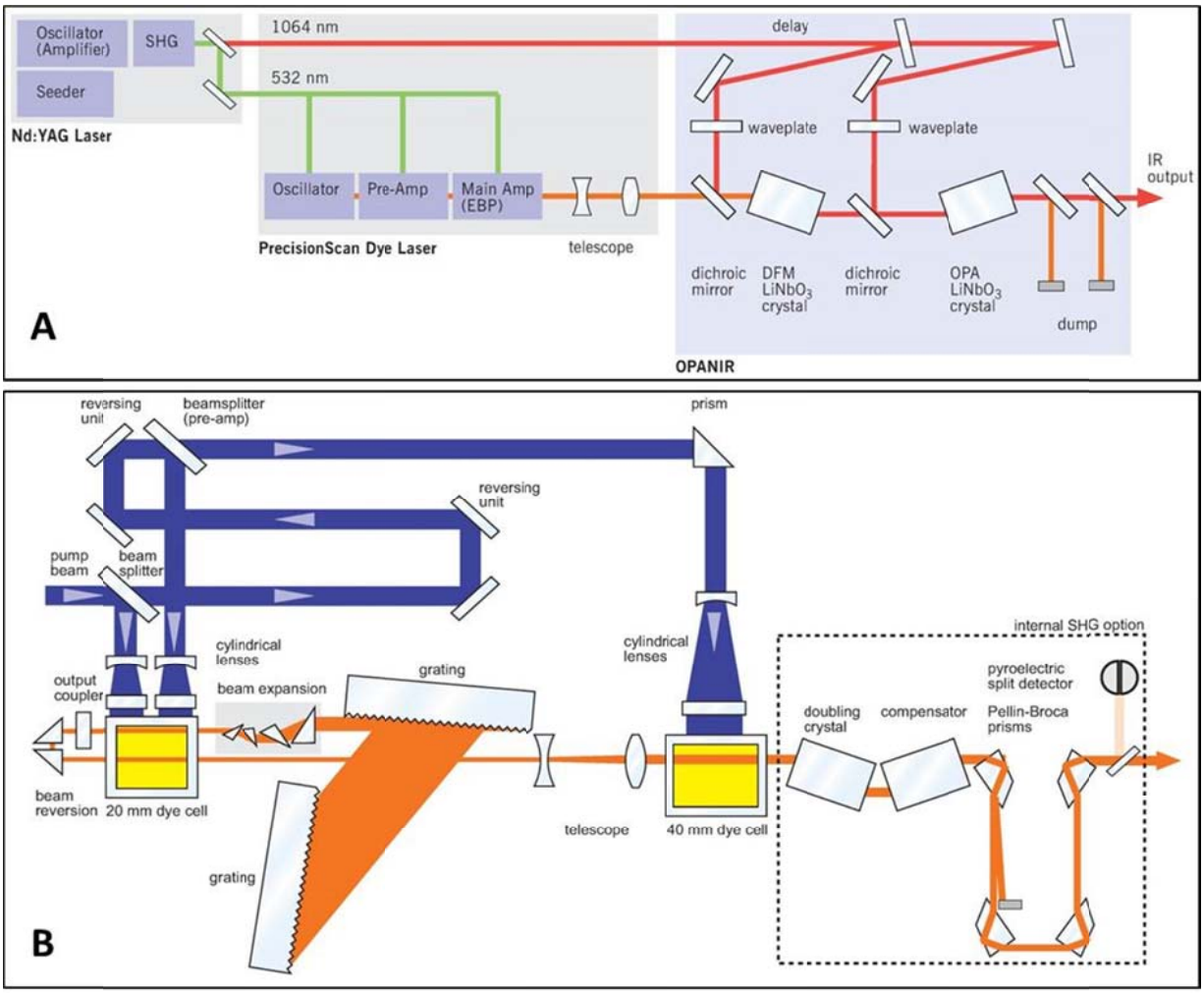

Figure 2) A - *Laser system manufactured by Sirah. SHG: second harmonic generator, EBP: enhanced beam profile cell, DFM: difference frequency mixing, OPA: optical parametric oscillator.* **B -** *Detailed scheme of the dye laser and of the optional SHG.*

During the experimental campaign of Stromboli, BILLI has worked with two wavelengths and their relative absorption coefficients. See Table 2 [5].

Mode	Wavelength [nm]	Wavenumber [cm^{-1}]	CO_2 Abs. Coeff. [m^{-1}]
ON	2009.5369	4976.271	1.934
OFF	2008.4838	4978.880	0.3016

N.B.
- $\lambda_{ON} = 2008.4838\ [nm] \rightarrow minimum\ CO_2\ absorption$
- $\lambda_{OFF} = 2009.5369\ [nm] \rightarrow maximum\ CO_2\ absorption$

Table 2) *Wavelengths, Wavenumbers and CO_2 Absorption Coefficients calculated at STP (T=296K, P=1atm) [5].*

In fact, the main goal was to evaluate the exceedance of in-plume CO_2 concentration; for this reason the system has worked in DIAL mode of operation.
On this regard, it is noted that [1,2,3]:

- the system is able to explore the atmosphere in both vertical and horizontal directions;
- each lidar profile is obtained averaging 100 shots ON and OFF (interleaved between them with $t_{shift} \sim 0.1\ s$);
- the temporal resolution between laser shots – Δt is equal to 10 ns, with a range (spatial) resolution – ΔR of 1.5 m;
- a concentration profile is obtained (20 s) by a couple of lidar signals (ON and OFF) using the newly designed mathematical technique named BRIDGE DIAL;
- starting from lidar signals of the same scan it is possible to retrieve the dispersion map of in-plume CO_2 concentration [ppm] in the investigated area;
- knowing the (estimated) plume speed it is possible to obtain the CO_2 flux [Kg/s].

The system could also be used for the measurement of wind speed [6], thanks to the ability of steering the optics in different directions. The number of photons backscattered by the atmosphere at a given distance from the instrument is proportional to the backscattering coefficient. This factor is a function of the density of aerosols responsible for the light scattering. Any change in its spatio-temporal distribution during a data acquisition will lead therefore to variations in the lidar returns from one laser shot to another. In particular, a wind flow along the beam axis will be detected from the transport of the spatial inhomogeneities of the backscattering coefficient along the optical path.

Moreover, the laser source chosen for BILLI has some remarkable features [1,2,3]:

1. 10 pm stability corresponding to about 0.2 cm^{-1} stability;
2. enhanced beam profile amplifier (EBPA);
3. dynamic mode option (DMO);
4. piezo wavelength control (PWC);

EBPA: the circular cross section of the amplifier cells inside the dye laser supports an improved quality of the beam profile: near-Gaussian intensity distribution in the far field is obtained, thus implying circular profile, small size and low divergence.

DMO: the longitudinal mode spacing of the dye laser resonator is 0.018 cm^{-1}. Its linewidth is 1.2 pm which corresponds to about 0.025 cm^{-1}. This means that two longitudinal modes will be emitted. Unfortunately, the mode structure is not predictable nor constant over minutes: this means that during a lidar experiment energy could distributed in unknown and unequal parts in the two modes, causing a serious problem due to the narrow bandwidth of the CO_2 absorption lines. In order to overcome this difficulty, dynamic mode option (patent pending) has been developed: a piezo changes the resonator length of the dye laser between every shot, thus modifying the longitudinal

mode structure for successive laser pulses. Hence the spectral shape for successive laser pulses is statistically distributed (in our case 50% of the energy is emitted in each mode) and artifacts due to the longitudinal mode structure are suppressed.

PWC: piezo wavelength control allows the laser system to fire at ON and after 1/10 of second at OFF. This is achieved as follows:

- the rotatable Littrow grating of the dye laser is mounted on a tilt piezo changing the wavelength between successive Nd:YAG laser shots so that one shot is fired at ON and the other one at OFF (Figure 3 - A);
- although the piezo is fast enough for a 10 Hz repetition rate, the nonlinear crystals inside the DFM and OPA cannot be moved so fast; therefore two more nonlinear crystals have been mounted, the first one after the standard DFM crystal and the second one after the standard OPA crystal; these two new crystals have been mounted with a slightly different angle in order to produce OFF: this is achieved by a special mechanics allowing the adjustment of the new crystal to the slightly different angle with a micrometric screw (Figure 3 - B).

The visible and UV emissions of the system could be used for the spectroscopic measurement of other species (e.g. SO_2, another key molecule of volcanic plumes).
Furthermore, it has been noticed that the measurement error was dominated by instability in wavelength setting. This is why it was implemented a photo-acoustic cell filled with pure CO_2 at atmospheric pressure and temperature, close to the laser exit, as shown in Figure 3 - C. Using new software developed for this application, it is possible to change the transmitted wavelength (by moving the stepper motor inside the resonator cavity of the dye laser) and to record the photo-acoustic signal (averaging 10 laser shots, corresponding to 1 s). Once corrected the wavelength displayed by the laser controller for a small shift (0.12 cm^{-1}), the agreement between experiment and theory [7] is excellent, i.e. within the laser linewidth (0.04 cm^{-1}) (Figure 3 - D). In practice, the wavelength can be controlled by recording the photo-acoustic signal before each atmospheric measurement and the experimenter can set the ON and OFF wavelengths with accuracy better than the laser linewidth.

Summarizing, the system has some special features reported in Figure 3 [1,2,3]:

- enhanced beam profile amplifier (beam size/divergence);
- dynamic mode option (spectral stability);
- piezo wavelength control (ON-OFF transition);
- double crystals (ON-OFF generation/amplification);
- photo-acoustic cell filled with CO_2
- mechanical control of telescope mirrors (by means of LABVIEW routines) in both horizontal and vertical plane.

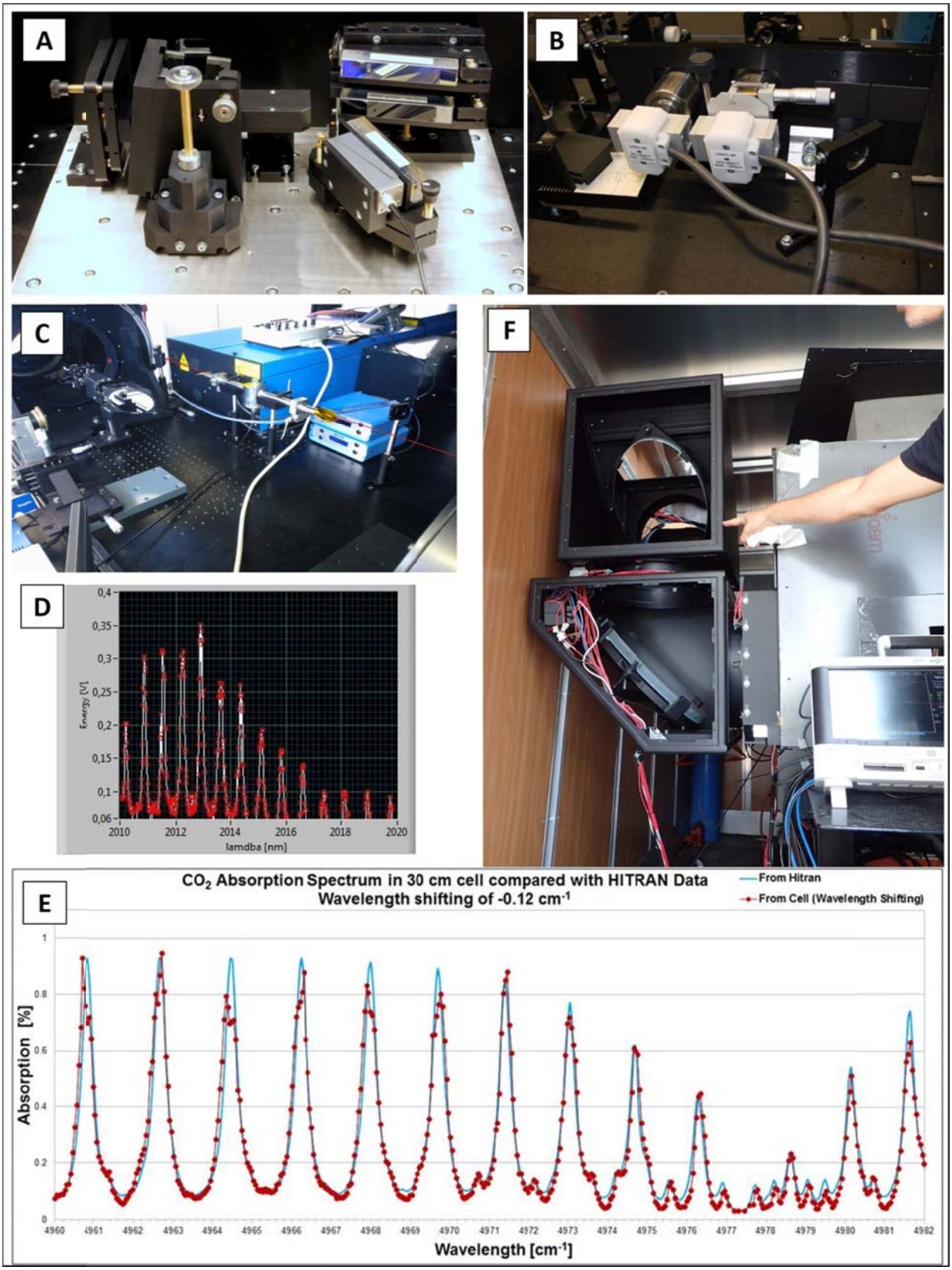

Figure 3) Special *Features of the system:* **A** *– Double Grating (Grazing Incidence: 2400 lines/mm),* **B** *- Piezo Wavelength Control,* **C** *- Photo-acoustic cell (inside the white circle),* **D** - Photo-acoustic signal from the cell, **E** *- Theoretical (line) and experimental (circles and line) CO_2 absorption spectrum.,* **F** - The experimenter arm indicates the two large elliptical mirror inside their precision motorized turning mount (opened). The box behind the experimenter contains lasers and telescope.

2.2 The BRIDGE DIAL technique

The lidar system principle of operation is simple: the backscatterers (molecules and aerosols) at the distance R from the system send back part of the laser pulse toward the active surface of the telescope. Consequently, the analysis of the detected signal as a function of t, time interval between emission and detection, allows one to study the chemico-physical properties of the atmosphere along the beam, since the simple relation between t and R is given by R=c·t/2, where c is the speed of light.
In its round trip, the laser pulse is attenuated by the atmosphere. This phenomenon is quantified by the extinction coefficient of the probed air that is linked to the absorption of its gases. Usually their absorption bands are narrow and this property can be used to measure their concentration by DIAL: this system is based on the detection of backscattered photons from laser pulses transmitted to the atmosphere at two different wavelengths. At one wavelength (OFF), the light is almost only scattered by air molecules and aerosols, whereas at the other one (ON), it is also absorbed by the species under study. The difference between the two recorded signals is thus related to the gas concentration. In this way, it is possible to retrieve the concentration profile along the laser beam [5,6].

The Lambert-Boguert-Beer law relates the attenuation of light to the properties of the material through which the light is traveling. It stated that absorbance of a material sample is directly proportional to its thickness (path length). From this law it is possible to obtain the attenuation coefficient (α) of a material sample (e.g. the atmosphere):

$$I_1 = I_0 \cdot e^{-2 \cdot \alpha \cdot l} \tag{1}$$

with:
I_1: $output\ intensity\ of\ signal\ transmitted\ by\ the\ surface/medium$
I_0: $input\ intensity\ of\ signal\ received\ by\ the\ surface/medium$
α: $global\ attenuation\ coefficient\ of\ the\ medium$
$NB) the\ attenuation\ coefficient\ is\ related\ to\ the\ attenuation\ cross\ section\ and\ to\ number\ density\ of\ the\ attenuating\ specie\ in\ the\ material\ sample\ as: \alpha = \sigma \cdot N$
$l\ or\ R$: $thickness\ or\ path\ lenght\ of\ the\ medium$

Since the system works in DIAL mode (Differential Absorption Lidar), each profile is composed of two signals; they are acquired, respectively, at ON (CO_2 maximum absoprtion) and OFF wavelength (CO_2 minimum absorption). Furthermore, from the fieldwork experience at Stromboli, it is known that the laser beam was backscattered several times by the plume and by the rockface and the system has worked, for the first time, over long distances up to 3 Km. For these reasons, the lidar profile processing was splitted in two portions.
With regard to the Figure 4, it is possible to see an example of lidar profile from the position of the system until 2 Km. There are two visible peaks (particularly at OFF wavelength), the first one corresponds to I_0^{off} and it is the signal due to the scattering, inside the laboratory, of some photons of the transmitted laser pulse (this peak gives the exact time of pulse transmission and is proportional to the transmitted energy, thus providing the signal normalization). Instead, the second peak corresponds to I^{off}; this is the lidar signal from the rockface of volcanic crater named "Pizzo".
Moreover, in Figure 5, there is a zoom of the lidar profile number 8 (from 1500 to 3500 m) that belongs to the first loop of a morning scan acquired the 26 of June, 2015. In this picture, it is possible to distinguish two peaks referred to lidar signal from the rockface and, in particular, to the edges of Stromboli volcanic crater. They are named, respectively: "Pizzo" (I_0^{off}) and "Vancori" (I^{off}) by volcanologists.

Therefore, first of all, the two transmittances related to ON/OFF signals are computed, then it is possible to evaluate the ratio between these two elements:

$$\frac{I^{off}}{I_0^{off}} = e^{-2\cdot\alpha_{off}\cdot R} \qquad and \qquad \frac{I^{on}}{I_0^{on}} = e^{-2\cdot\alpha_{on}\cdot R} \tag{2}$$

$$\frac{\frac{I^{off}}{I_0^{off}}}{\frac{I^{on}}{I_0^{on}}} = \frac{T_{off}}{T_{on}} = \frac{e^{-2\cdot\alpha_{off}\cdot R}}{e^{-2\cdot\alpha_{on}\cdot R}} = e^{-2\cdot\sigma_{off}\cdot N\cdot R}\cdot e^{+2\cdot\sigma_{on}\cdot N\cdot R} \rightarrow e^{2\cdot(N\cdot D)\cdot\Delta\sigma} \tag{3}$$

From the equation (3), it is possible to obtain the average concentration of the investigated chemical species (e.g. carbon dioxide – CO_2) between the two peaks and in both cases already mentioned:

- *Average CO_2 concentration between Laboratory Peak and Pizzo*

$$\bar{N}_{lp} = \left[\frac{1}{2\cdot\Delta\sigma\cdot D_{lp}}\cdot \ln\frac{T_{off-lp}}{T_{on-lp}}\right] \tag{4A}$$

- *Average CO_2 concentration between Pizzo and Vancori*

$$\bar{N}_{pv} = \left[\frac{1}{2\cdot\Delta\sigma\cdot D_{pv}}\cdot \ln\frac{T_{off-pv}}{T_{on-pv}}\right] \tag{4B}$$

with:

$\Delta\sigma\ [m^{-1}] = \sigma_{ON} - \sigma_{OFF}$, *con* $\sigma_{on/off}$ CO_2 *absorption cross sections at* $\lambda_{on/off}$

$D_{lp/pv}\ [m] =$ *peaks range* $(Lab.Peak - Pizzo\ and\ Pizzo - Vancori)$

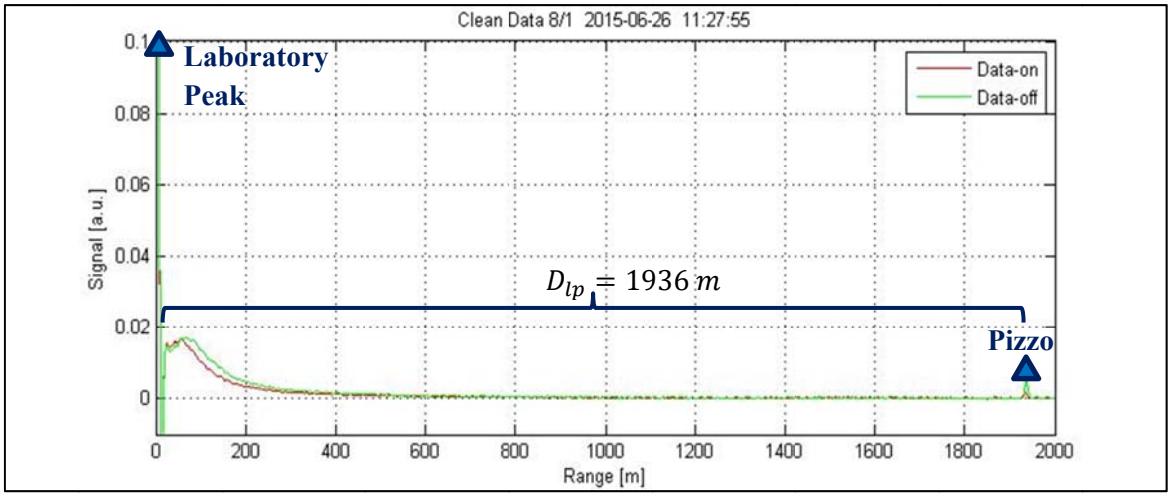

Figure 4) *Clean Data. Particular of Laboratory Peak and Pizzo.*

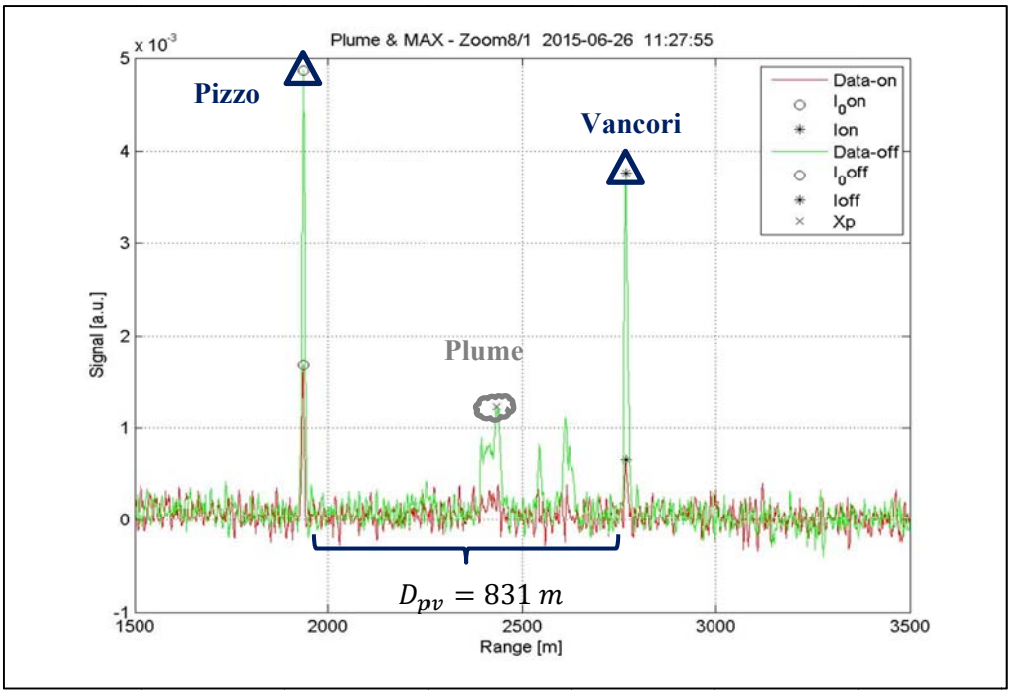

Figure 5) *Clean Data. Pizzo, Plume and Vancori*

After the smoothing of the analyzed lidar profile (with span equal to 13 – 19.5 m, taking into account a spatial resolution of 1.5 m), the second step consists of the evaluation of the Range Corrected Signal – $S(R)_{on/off}$ for both ON and OFF clean data. This procedure is carried out only for the portion of the signal included between 1500 and 3500 m, in which is higher the probability to find plume. On this regard, see Figures 6 and 7. From the equation below:

$$S(R)^{tot}_{on/off} = \ln(data^{*}_{on/off} \cdot R^2) \tag{5}$$

with: $data^{*}_{on/off} = data_{on/off} - bkgnd_{on/off},\ con\ bkgnd_{on/off} = \min(data_{on/off})$

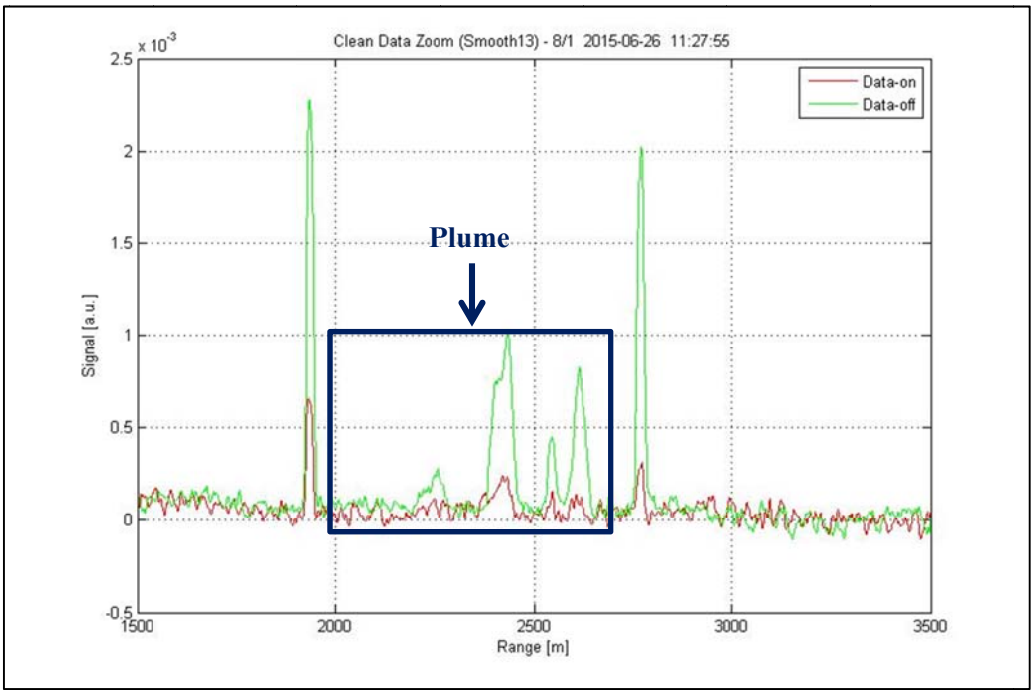

Figure 6) *Clean data with plume trace after the smoothing method (span=13). Zoom between 1500 and 3500 m*

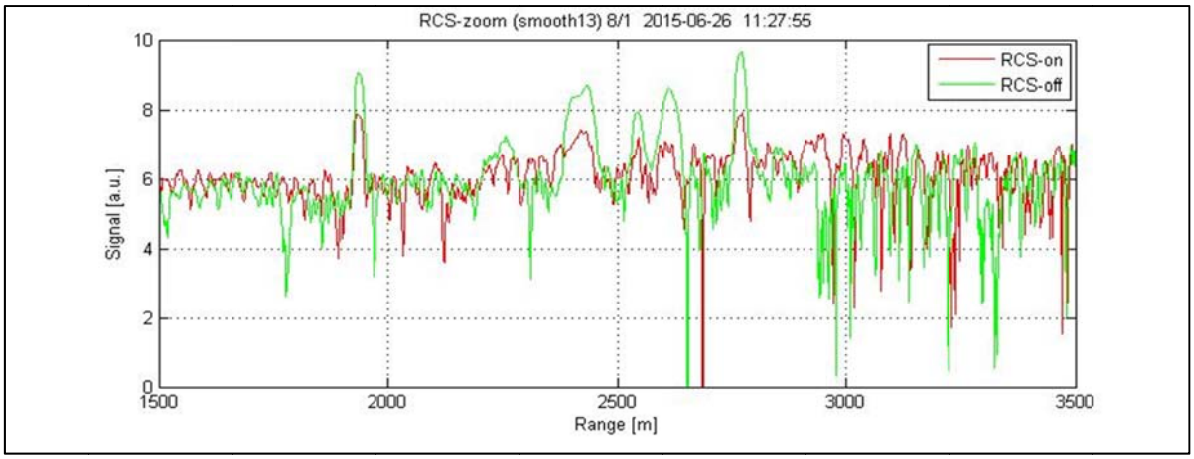

Figure 7) *RCS computed from 1500 to 3500 m*

Therefore, can be evaluated the in-plume CO_2 concentration between the two peaks named, respectively, Pizzo and Vancori.
Using the Range Corrected Signal (5) related to the OFF wavelength (because the OFF signal is higher than ON signal) and assuming that the average CO_2 concentration (4B) is proportional to the RCS, it is possible to retrieve the effective presence of in-plume CO_2 concentration, known as the exceedance of in-plume CO_2 concentration (Figure 8). By means of the equations (6) and (7):

$$C = C_0 + \Delta C \cdot S_i \ [ppm]\ Global\ in-plume\ CO_2\ concentration \tag{6}$$

$$C_{exc} = C - C_0 \ [ppm]\ Exceedance\ of\ in-plume\ CO_2\ concentration \tag{7}$$

$$NB)\ C_{exc}\ represent\ the\ real\ in-plume\ CO_2\ concentration\ without\ the\ carbon\ dioxide\ natural\ background\ value.$$

with:

- $\Delta C = \frac{[(N-C_0)\cdot D]}{\Delta R \cdot \sum_i S_i}$
- $D[m] = plume\ basis\ between\ the\ two\ peaks\ (Pizzo\ and\ Vancori)$
- $C_0 = \bar{N}_{lp}\ [ppm]\ \ Average\ CO_2\ concentration\ \ for\ clean\ atmosphere\ (between\ Lab\ Peak\ and\ Pizzo), as\ already\ mentioned\ in\ equation\ (4B).$
- $N = \bar{N}_{pv}\ [ppm]\ \ Average\ CO_2\ concentration\ with\ plume\ (between\ Pizzo\ and\ Vancori)$
- $\Delta R = 1.5\ [m]\ spatial\ resolution\ of\ the\ system$
- $S_i\ e\ \sum_i S_i\ \ they\ are, respectively, the\ signal\ points\ and\ the\ sum\ of\ signal\ (\ RCS^{OFF}) points\ evaluated\ inside\ the\ plume.$

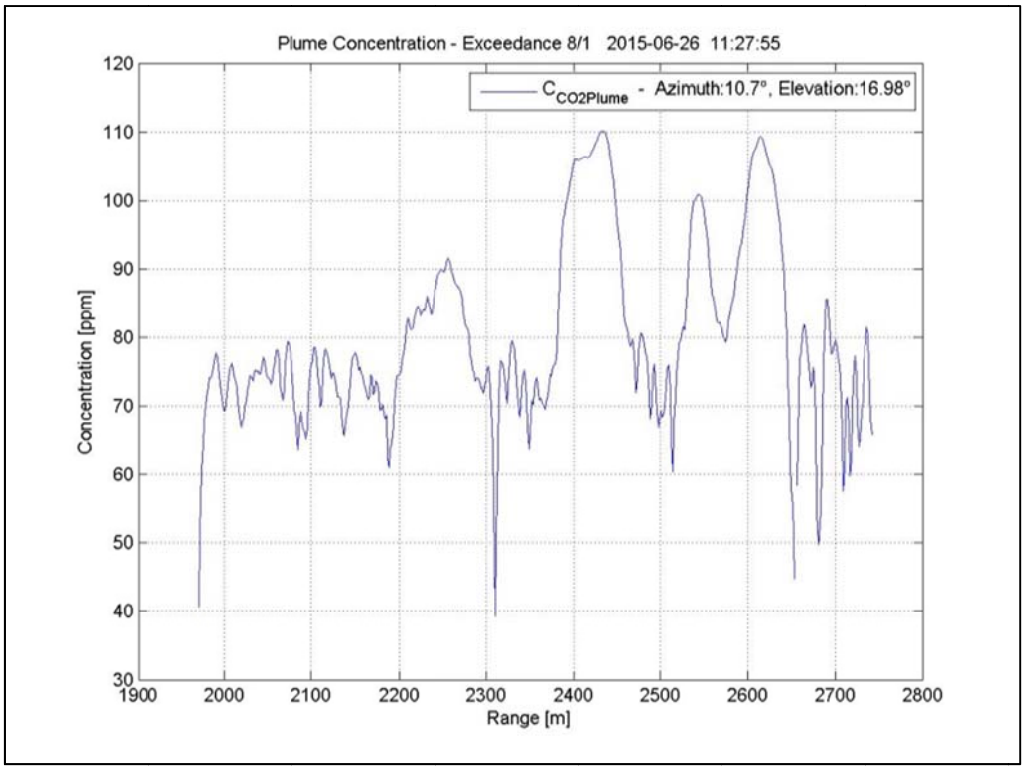

Figure 8) *Exceedance of in-plume CO_2 concentration evaluated for RCS.*

The last step is the normalization of equation (7), subtracting the background value of in-plume CO_2 concentration. This coefficient is equal to 72.7 ppm and can be evaluated as the average value of in-plume CO_2 concentration trend from 1974 to 2188 m (inside this range the concentration profile of CO_2 is close to 0, so it is reasonable to assume that from this portion can be extrapolated the "background of plume"). Through this step, it is possible to obtain the correct value of exceedance in-plume carbon dioxide concentration:

$$C_{exc-corr} = C_{exc} - mean[C^*_{exc}] \tag{8}$$

$$with\ C^*_{exc}: exceedance\ of\ in-plume\ CO_2\ concentration\ from\ 1974\ to\ 2188\ m$$

For more details, see Figure 9.

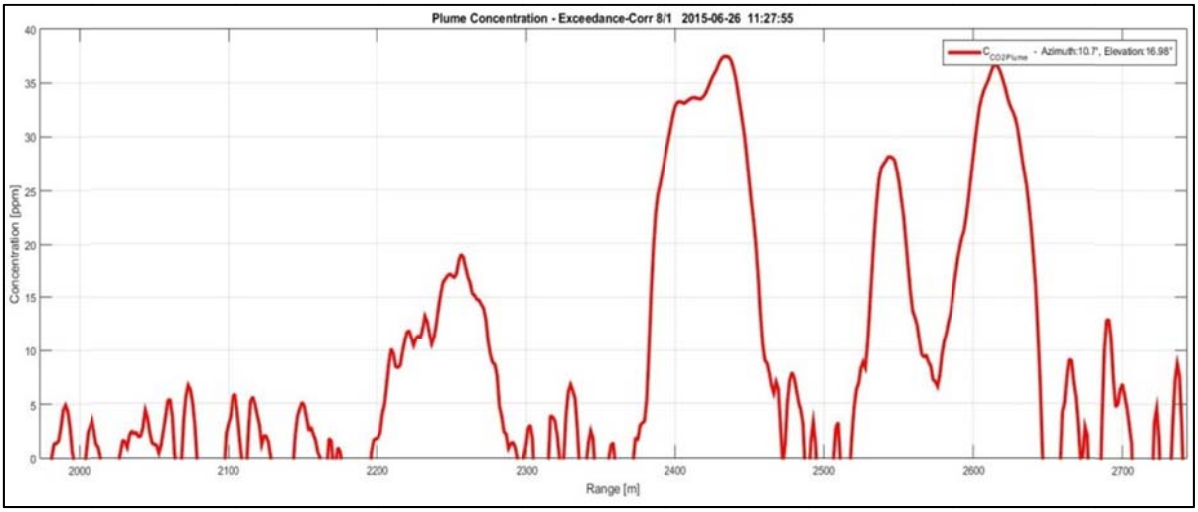

Figure 9) *Exceedance of in-plume CO_2 concentration after correction.*

3. The experimental campaign of Stromboli

In this section, both the experimental set-up of the BILLI DIAL system and the weather conditions of the investigated area, during the experimental campaign of Stromboli (24-29/06/2015), are discussed.

3.1 The experimental area

The experimental campaign of Stromboli has been carried out from the 24 to 29 of June, 2015. As shown in Figure 10 - A, Stromboli is a small island in the Tyrrhenian Sea, off the north coast of Sicily, containing one of the three active volcanoes in Italy. It is one of the eight Aeolian Islands (ME), a volcanic arc north of Sicily.
The main goal of the field campaign was the measurement of carbon dioxide contained in volcanic fumes, for early warning of eruptions.
For this purpose, BILLI was mounted in a small truck positioned far from the volcanic plume (up to 3 Km) and probed it with its laser beam (Figure 10 - B), without any risks for authorized personnel.
Thanks to two large elliptical mirrors (Figure 3 - F) the instrument field-of-view could be aimed to any direction. With such configuration, and scanning the plume in both horizontal and vertical planes, the CO_2 concentrations outside and inside the volcanic plume were measured. These measurements, once carried out over a significant part of the plume, and upon scaling to the transport rate (as derived from the wind speed at the plume altitude), allowed one to retrieve also the carbon dioxide flux.
In-situ calibration of the system has been possible thanks to a fixed reference point: a little building, named "Casuzza" by volcanologists, placed 930 m from the position of the system. This reference point was particularly useful during the data post-processing step, so as to convert experimental Azimuth angles into real Azimuth angles. In fact, once georeferencing this point, thanks to Google earth software [8], it has been possible to determine both the exact position of the system and the main orographic obstacles in the investigated area and, therefore, their relative geographic coordinates.
As it is shown in Figure 10 – B, BILLI DIAL system has scanned the area of interest in both vertical (Elevation angles from 14° to 24°) and horizontal planes (Azimuth anlges from 227° to 317°).

Figura 10) A – *Map of Eolian Islands – Detail of Stromboli volcanic island.* **B –** *Map of the experimental area and main orographic obstacles.*

The most of scan have been done along the vertical direction, for a fixed Azimuth angle. This angle corresponds to the system's LOS that intercepted the rockface of volcanic crater named "Vancori".
In particular, the most common configuration was: Azimuth angle – 237.8° ("Vancori"); Elevation angles – from 16.7° to 20.66° (with each step equal to Δ=0.04°).
Moreover, during the experimental campaign, it has been noticed that for elevation angles greater than 17.6°, the system's LOS overtook Vancori's peak; instead, for Elevation angles greater than 17° the system's LOS overtook Pizzo's side; finally, for Elevation angles included between 17° and 17.6° it has been possible to detect these two orographic obstacles and, in some cases, also plume traces. This was true for a fixed value of Azimuth angle, equal to 237.8°.
These informations were really useful for the analysis and processing of data acquired during the measurement sessions.
For more details, see Figure 11 in which are reported the thresholds of Elevation angles previously mentioned.

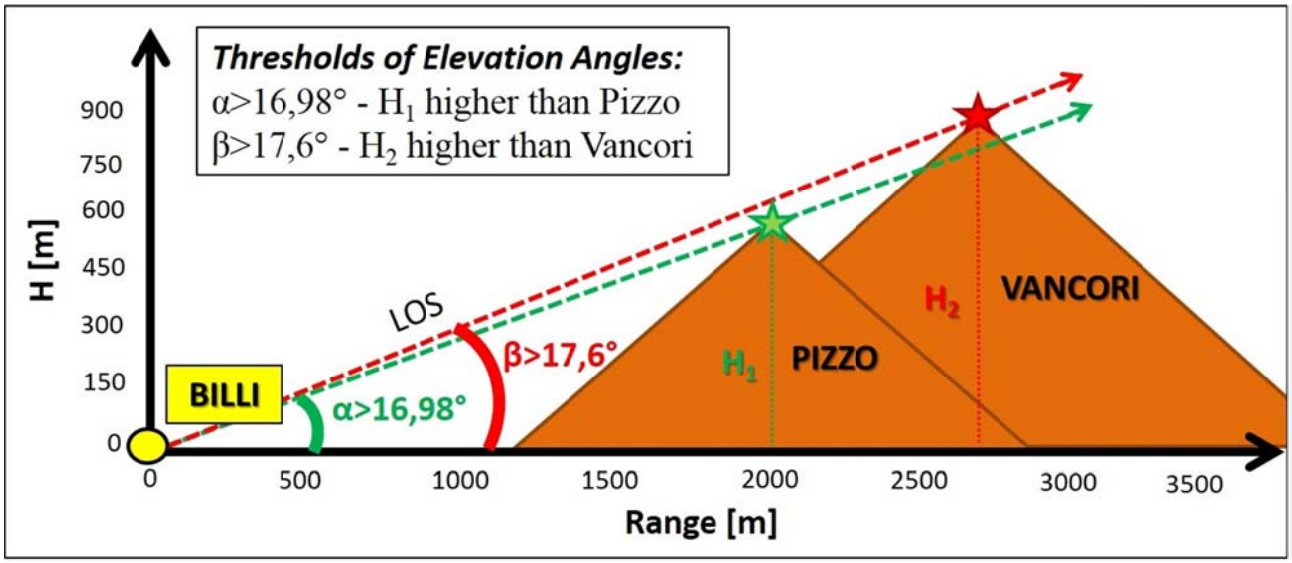

Figure 11) *Sketch of thresholds of elevation angles.*

3.2 Meteorological parameters

This paragraph reports the trends of the main meteorological parameters, concerning the measurement sessions (24-29/06/2015) of the experimental campaign of Stromboli.
As it is known, the weather conditions strongly influence remote sensing systems and, therefore, also lidar measurements.
In particular, here the attention is focused on the analysis of the following parameters:

- Temperature [°C];
- Relative Humidity [%];
- Precipitations [mm];
- Wind Speed [Km/h];
- Wind Direction [°].

On the basis of field inspections, carried out during the measurement sessions, and correlating the experimental data with weather trends, extrapolated by several forecast websites [9], it is possible to prove that the weather conditions during the experimental campaign were fine. In fact, the weather was sunny and warm, with typical values of temperature of the Mediterranean climate and the total absence of precipitations. This fact, has significantly favored in-situ measurements.
In Tables 3 and 4, are reported, respectively, the most important monthly and weekly meteorological trends; such as:

- The monthly/weekly average temperature;
- The monthly/weekly average relative humidity;
- The monthly/weekly average precipitations;
- The monthly/weekly average wind speed/direction.

Moreover, in Tables 5 and 6 there is a comparison between annual (average) meteorological trends extrapolated by a forecast website [9] and monitored by in-situ weather stations of Italian Air Force at Stromboli and Messina [10].

The cross comparison analysis between different data has allowed to verify the reliability of trends reported in Tables 3 and 4.

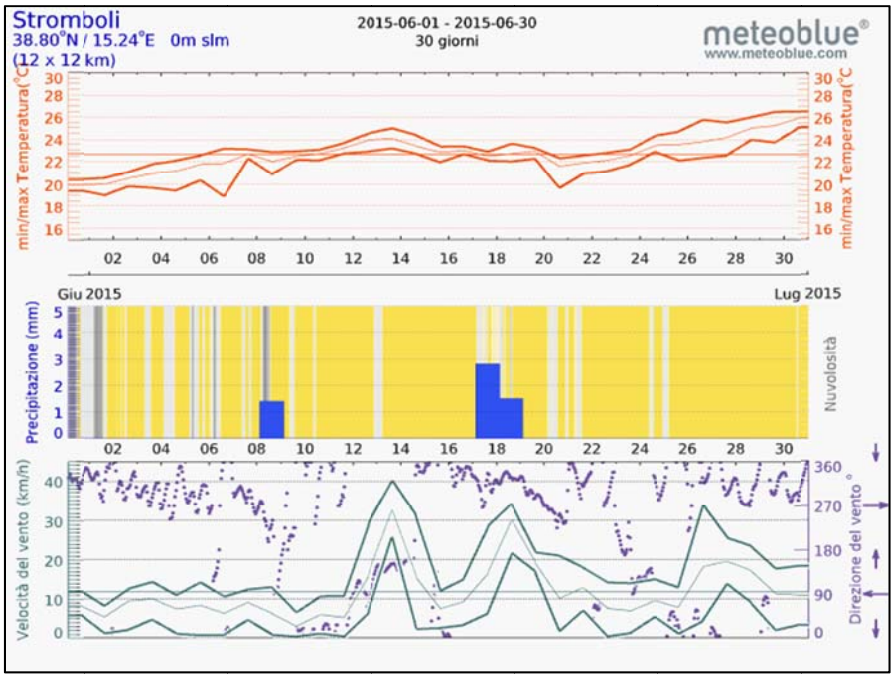

Table 3) *Meteorological parameters of Stromboli islands – monthly trends, June 2015.*

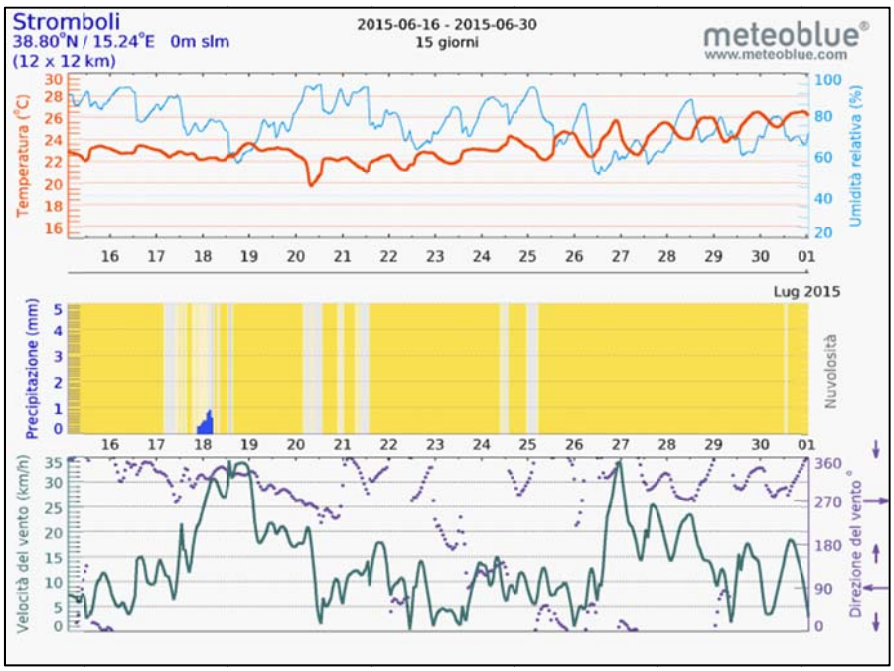

Table 4) *Meteorological parameters of Stromboli islands – weekly trends, June 2015.*

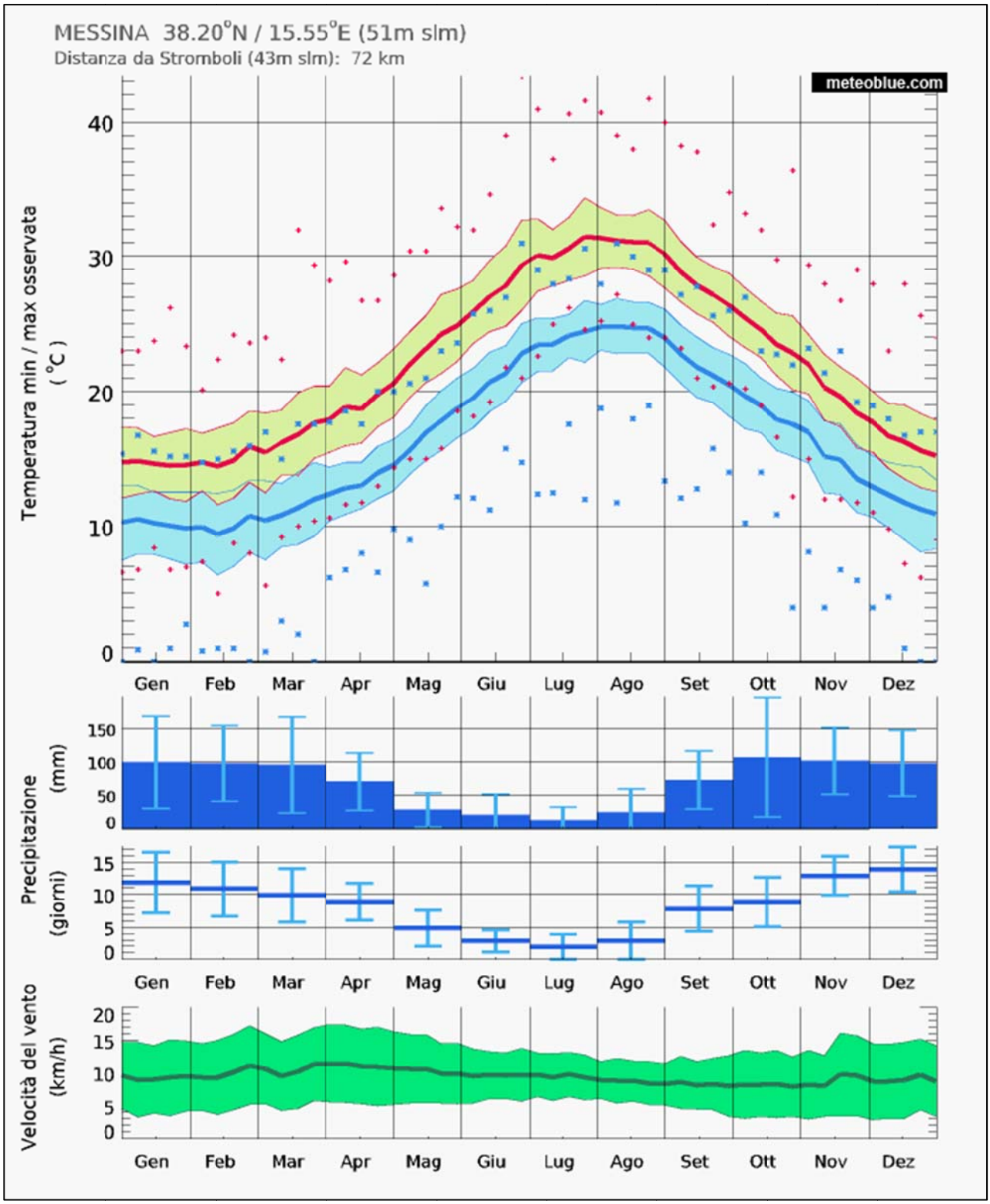

Table 5) *Annual weather trends and comparison between atmospheric conditions of Messina and Stromboli.*

Isola di Stromboli (1951-1980)	Mesi												Stagioni				Anno
	Gen	Feb	Mar	Apr	Mag	Giu	Lug	Ago	Set	Ott	Nov	Dic	Inv	Pri	Est	Aut	
T. max. media (°C)	14,8	15,0	15,9	18,4	22,2	26,2	29,3	30,2	27,9	23,6	19,6	16,4	15,4	18,8	28,6	23,7	21,6
T. min. media (°C)	9,8	9,5	10,3	11,9	14,8	18,4	21,1	21,8	20,1	16,6	13,7	11,3	10,2	12,3	20,4	16,8	14,9

MESSINA (1971-2000)	Mesi												Stagioni				Anno
	Gen	Feb	Mar	Apr	Mag	Giu	Lug	Ago	Set	Ott	Nov	Dic	Inv	Pri	Est	Aut	
T. max. media (°C)	14,4	14,7	16,1	18,3	22,5	26,8	30,0	30,5	27,5	23,2	18,8	15,8	15,0	19,0	29,1	23,2	21,6
T. min. media (°C)	10,1	9,8	10,9	12,5	16,4	20,4	23,4	24,2	21,5	17,8	14,1	11,6	10,5	13,3	22,7	17,8	16,1
T. max. assoluta (°C)	24,6 (1979)	25,8 (1979)	23,2 (1989)	29,0 (1985)	32,4 (1994)	40,1 (1982)	43,6 (1998)	40,2 (1994)	38,2 (1988)	36,4 (1999)	26,8 (1985)	24,4 (2000)	25,8	32,4	43,6	38,2	43,6
T. min. assoluta (°C)	2,0 (1999)	3,0 (1986)	0,7 (1987)	6,0 (1997)	10,0 (1987)	13,4 (1971)	16,0 (1974)	16,8 (1972)	12,8 (1971)	8,8 (1974)	5,2 (1975)	4,0 (1991)	2,0	0,7	13,4	5,2	0,7
Giorni di calura ($T_{max} \geq 30$ °C)	0	0	0	0	0	3	16	20	3	0	0	0	0	0	39	3	42
Giorni di gelo ($T_{min} \leq 0$ °C)	0	0	0	0	0	0	0	0	0	0	0	0	0	0	0	0	0
Precipitazioni (mm)	102,9	100,2	83,4	68,3	33,8	12,7	20,0	25,6	63,9	113,7	119,5	102,9	306,0	185,5	58,3	297,1	846,9
Giorni di pioggia	11	10	9	9	4	2	2	3	6	9	11	11	32	22	7	26	87
Giorni di nebbia	0	0	0	0	0	0	0	0	0	0	0	0	0	0	0	0	0
Umidità relativa media (%)	73	71	69	68	67	64	64	66	69	71	74	73	72,3	68	64,7	71,3	69,1

Table 6) *Official climate trends – weather stations of Italian Air Force at Stromboli and Messina.*

In conclusion, weather conditions did not significantly affect BILLI system measurements, except for a moderate influence of the wind that blew from northwest (in particular between the 27 and the 28 of June) and could probably scatter volcanic particles and fumes in the direction of the sea. However, weather conditions allowed also a quite good correlation between the detected lidar signals with the data collected by conventional in-situ instruments.

4. Results and discussion

In this section, the results of the experimental campaign of Stromboli are reported and thoroughly analyzed.
Data processing and interpretation is the last step of work and consists of the application of a newly designed DIAL method (for more details, see chapter 2.2). This is due to the intensity of lidar profiles, detected during the field campaign, was lower than common signals previously studied. For this reason it was impossible to use the classical DIAL method.
However, data processing can be divided into three phases:

1) *Data Classification*: consists in the rearrangement of raw lidar data and identification of plume signals;
2) *Data Processing*: elaborations of lidar data with the "BRIDGE DIAL Technique";
3) *Graphic Presentation*: productions of plots for data analysis and post processing steps.

On this regard, see Figure 12 (A-B).
As already stressed, the main goal of the work was the measurement of CO_2 in volcanic plumes for early warning of eruptions. For this purpose, Matlab scripts are specifically developed for data processing and graphic presentation of both CO_2 concentration profiles (real time application) and dispersion maps (in the post processing step).

A)

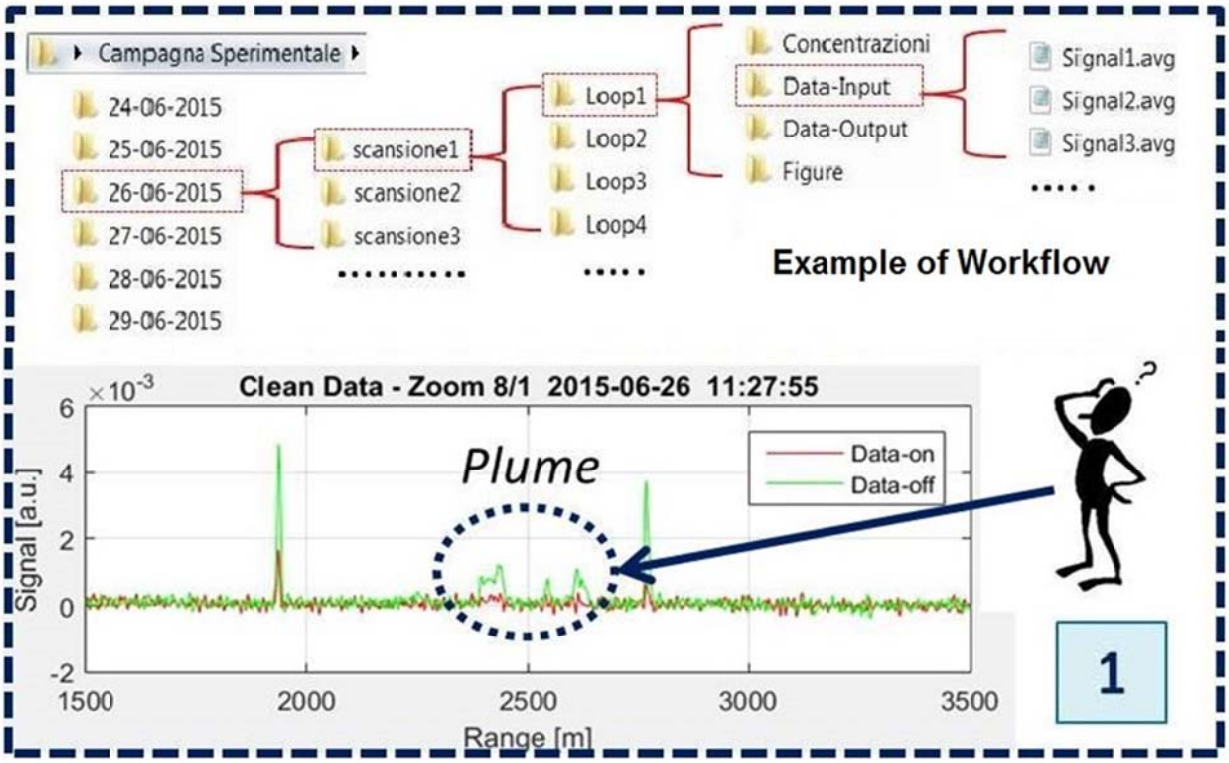

B)

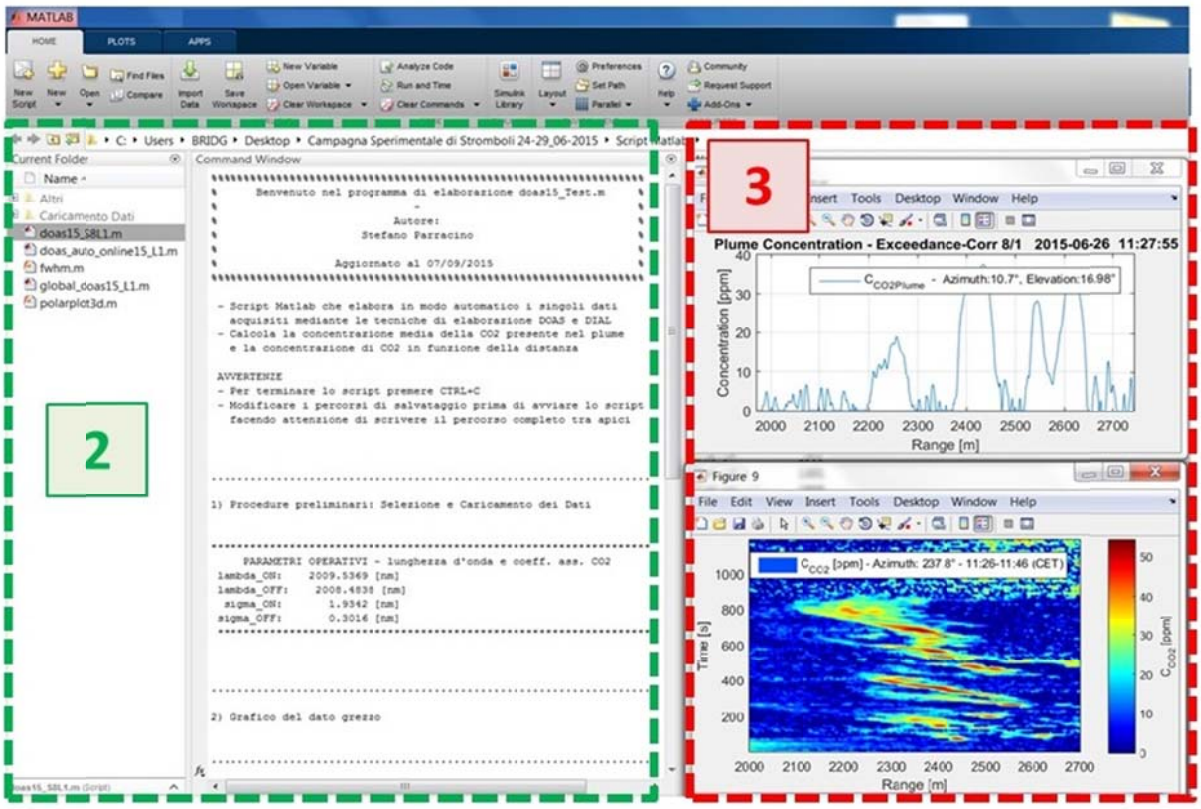

Figure 12) A - *Example of workflow and identification of raw signal,* **B** *– Example of screenshot during the data processing step.*

Moreover, the attention was focused on the experimental area (Figure 10 – B) and, therefore, the portion of lidar signals included between 1500 to 3500 m from the position of the system.
In particular, between Pizzo and Vancori rockfaces was higher the probability to find plume traces. In fact, these traces have never been detected before the position of Pizzo's side (≈2 Km from the position of BILLI) and rarely after the position of Vancori's peak (farther than 3 Km from the position of the system). For further details see Sections 4.3 and 4.5.
Furthermore, in order to simplify the reading, results are classified using the order reported in Table 7. The most important cases have been highlighted with different colors. For example, green boxes with exclamation mark indicate the presence of clear plume traces, instead yellow boxes with asterisk indicate the presence of background noise (with potentially weak plume traces). Finally, grey boxes with slash indicate that nothing relevant has been detected.
As you can see in Table 7, each daytime measurement session is composed of several scans, each scan is composed of one or more loop and each loop is composed fixed number of lidar signals.
Please note that only figures and maps that show clear plume traces have been reported in the following chapters.

DATE	TIME SESSION	SCAN	TYPE	LOOP/SIGxL	POINTING INFO	NOTE
24/06/2015						
9 Scan - 12 Loop N° Scan Plume: 4 (3V+1H) N° Loop Plume: 7 (4V+3H)	16:34-16:42	altre	V	1/14	Az: 248,1° - El: 19,5°-20,8°	!
	16:42-16:46	plume davanti	V	2/31	Az: 248,1° - El: 17,5°-20,5°	!
	16:54-17:10	effetto plume 19-23 vert	V	1/83	Az: 247,6° - El: 19°-21,02°	!
	18:47	fianco montagna	A	1/1	/	/
	18:49	doppio fianco montagna	A	1/1	/	/
	19:02-19:03	doppio fianco montagna 2	A	1/2	/	/
	19:10-19:42	fianco montagna 2	A	1/4	/	/
	19:54-21:15	scansione orizzontale	H	3/26	El: 19,4° - Az: 248,6°- 253,6°	!
	21:44-21:53	prova serale	A	1/5	/	/
25/06/2015						
8 Scan - 24 Loop N° Scan Plume: 2 (H) N° Loop Plume: 18 (H)	11:17-11:48	mattina	A	1/35	/	/
	14:45-15:04	scansione orizzontale 1	H	1/101	El: 20,7° - Az: 241,1°-251,1°	*
	15:17-15:20	scansione verticael 1	V	1/15	/	/
	15:29-16:07	scansione verticale 2	V	1/193	Az: 237,8° - El: 16,8°-27,4°	*
	16:15-16:33	scan vert sopra eliporto	V	1/94	/	/
	17:28-17:38	casuzza	A	1/11	/	/
	17:43-22:38	scansione orizzontale 2	H	6/251	El: 20,3° - Az: 241,1°-251,1°	!
	23:26-09:16	scan orizzontale 3 notte	H	12/251	El: 20,3° - Az: 241,1°-251,1°	!
26/06/2015						
8 Scan - 35 Loop N° Scan Plume: 4 (3V+1H) N° Loop Plume: 13 (12V+1H)	10:21-10:52	scan oriz dopo calib cella	H	1/142	El: 20,7° - Az: 241,1°-251,1°	!
	10:57-11:20	vancori scan 1 verticale	V	1/116	Az: 237,8° - El: 16,7°-21,82°	!
	11:26-12:45	vancori scan 2 vert 4loop	V	4/100	Az: 237,8° - El: 16,7°-20,66°	!
	12:58-14:09	vancori scan 3 vert 4loop	V	4/90	Az: 237,8° - El: 16,7°-20,26°	*
	17:09-17:31	scansione verticale 4	V	1/125	Az: 237,8° °- El: 16,7°-21,02° (odd signals) Az: 251,4°- El: 16,7°-21,02° (even signals)	*
	17:44-20:18	scan vertical 5 sx vancori	V	7/111	Az: 235,3° - El: 15,2°-19,6°	*
	20:49-23:36	scan verticale 6 notte	V	10/90	Az: 237,8° - El: 16,7°-20,26°	*
	00:17-02:41	scan verticale 7 notte	V	7/111	Az: 237,8° - El: 15,2°-19,6°	!
27/06/2015						
5 Scan - 54 Loop N° Scan Plume: 0 N° Loop Plume: 0	10:26-10:43	scansione verticale 1	V	1/88	Az: 237,8° - El: 15,2°-18,68°	*
	10:57-13:35	scansione verticale 2	V	8/101	Az:237,8° - El:15,7°-19,7°	*
	14:56-17:47	scansione verticale 3	V	8/101	Az:237,8° - El:15,7°-19,7°	*
	19:21-22:39	scansione verticale 4	V	10/101	Az:237,8° - El:15,7°-19,7°	*
	00:13-09:44	scan verticale 5 notte	V	27/109	Az:237,8° - El:15,7°-20,02°	*
28/06/2015						
6 Scan - 59Loop N° S. PL.: 2 (V) N° L PL.: 43 (V)	10:58-11:15	scansione verticale 1	V	1/90	Az:237,8° - El:15,7°-19,26°	*
	11:30-15:37	scansione verticale 2	V	14/90	Az:237,8° - El:15,7°-19,26°	*
	15:41-15:59	scansione verticale 3	V	1/90	Az:237,8° - El:15,7°-19,26°	*
	17:18-18:12	scansione verticale 4	V	3/90	Az:237,8° - El:15,7°-19,26°	!
	18:49-23:49 (L1-17)	scansione verticale 5	V	17/90	Az:237,8° - El:15,7°-19,26°	!
29/06/2015	23:49-06:34 (L18-L40)	scansione verticale 5	V	23/90	Az:237,8° - El:15,7°-19,26°	!

TABLE CAPTIONS			
!	*Plume*	**V**	*Vertical Scan*
*	*Background noise (include weak plume traces)*	**H**	*Horizontal Scan*
/	*Nothing relevant*	**A**	*Anomalous Scan (fixed, oblique, etc.)*

N.B.

TOT n° of SCAN: 36 – TOT n° of LOOP: 184
TOT n° of SCAN with PLUME: 12 (8V+4H) – TOT n° of LOOP with PLUME: 81 (59V+22H)

Table 7) *Summary of data acquired during the experimental campaign of Stromboli (24-29/06/2015).*

Preliminary notes for the interpretation of CO_2 concentration scan figures

CO_2 concentration dispersion maps reported in this study are referred to vertical scan (as a function of range [m] – X axis, time [s] and elevation angle [°] – Y axis) and horizontal scan (as a function of range [m] – Y axis, time [°] and azimuth angle [°] – X axis). The color bar on the right of each figure is referred to the CO_2 concentration (expressed in term of [ppm]). Red, orange and yellow colors are used to indicate a strong variation of the exceedance of in-plume CO_2 concentration; instead, blue color usually represents the background noise.
Moreover, each figure caption reports: the carbon dioxide unit of measurement, the time slot referred to each measurement session (local civil time) and a fixed azimuth or elevation angle for, respectively, vertical or horizontal scan.

4.1 24/06/2015

During the measurement session of the 24 of June, 2015; a significant amount of in-plume CO_2 concentration traces have been detected in several scans. In particular, the attention is focused on:

- "Altre" – vertical scan, data acquired from 04:34 p.m. to 04:42 p.m. – Figure 14.
- "Plume davanti" – vertical scan, data acquired from 04:42 p.m. to 04:46 p.m. – Figure 15.
- "Effetto plume 19-23 verticale" – vertical scan, data acquired from 04:54 p.m. to 05:10 p.m. – Figure 16.
- "Scansione Orizzontale" – horizontal scan, data acquired from 07:54 p.m. to 09:15 p.m. – Figure 17.

Instead, in other scans nothing relevant has been detected.
For further details about the main characteristics of this session, reference is made to Table 7.

"Altre"

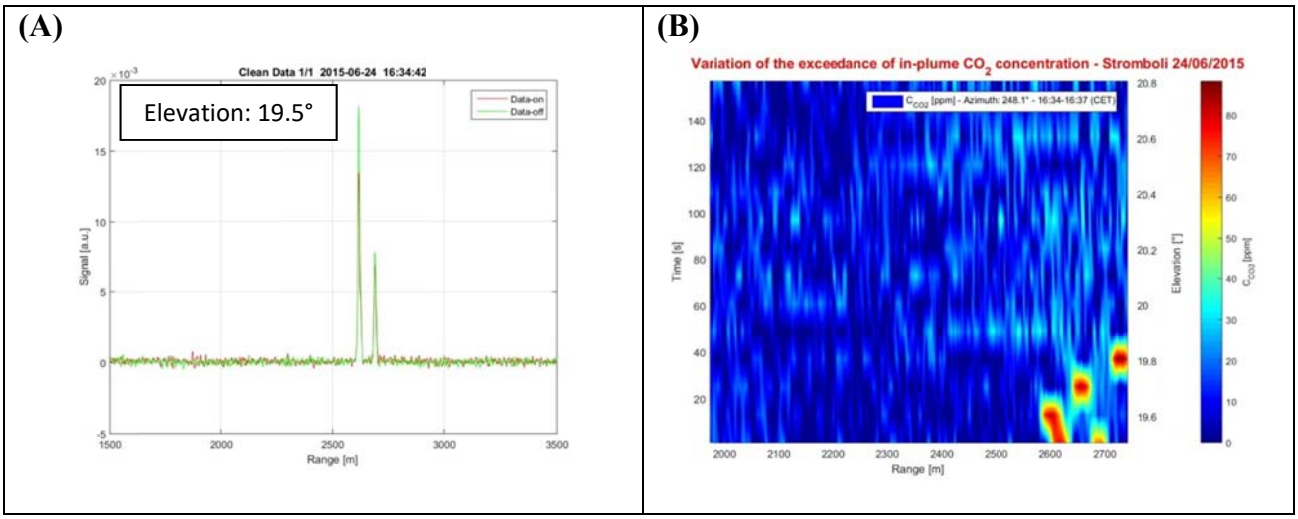

Figure 13) A – *Example of lidar profile containing CO_2 plume peaks between 2.5 Km and 3 Km.* **B –** *Vertical scan in Cartesian coordinates of the exceedance of in-plume CO_2 concentration as a function of range [m], elevation angle [°] and time [s]. It is possible to see plume traces in the bottom right corner of the map. A reasonable explanation of the high density of CO_2 spots could be due to an increase in relative humidity (thus, CO_2 molecules have been condensed into the atmosphere and their scattering properties have been increased), combined with the effect of the wind that have scattered the plume traces next to Vancori's peak.*
NB) LOS of the system was pointed on the right side of Pizzo.

"Plume davanti"

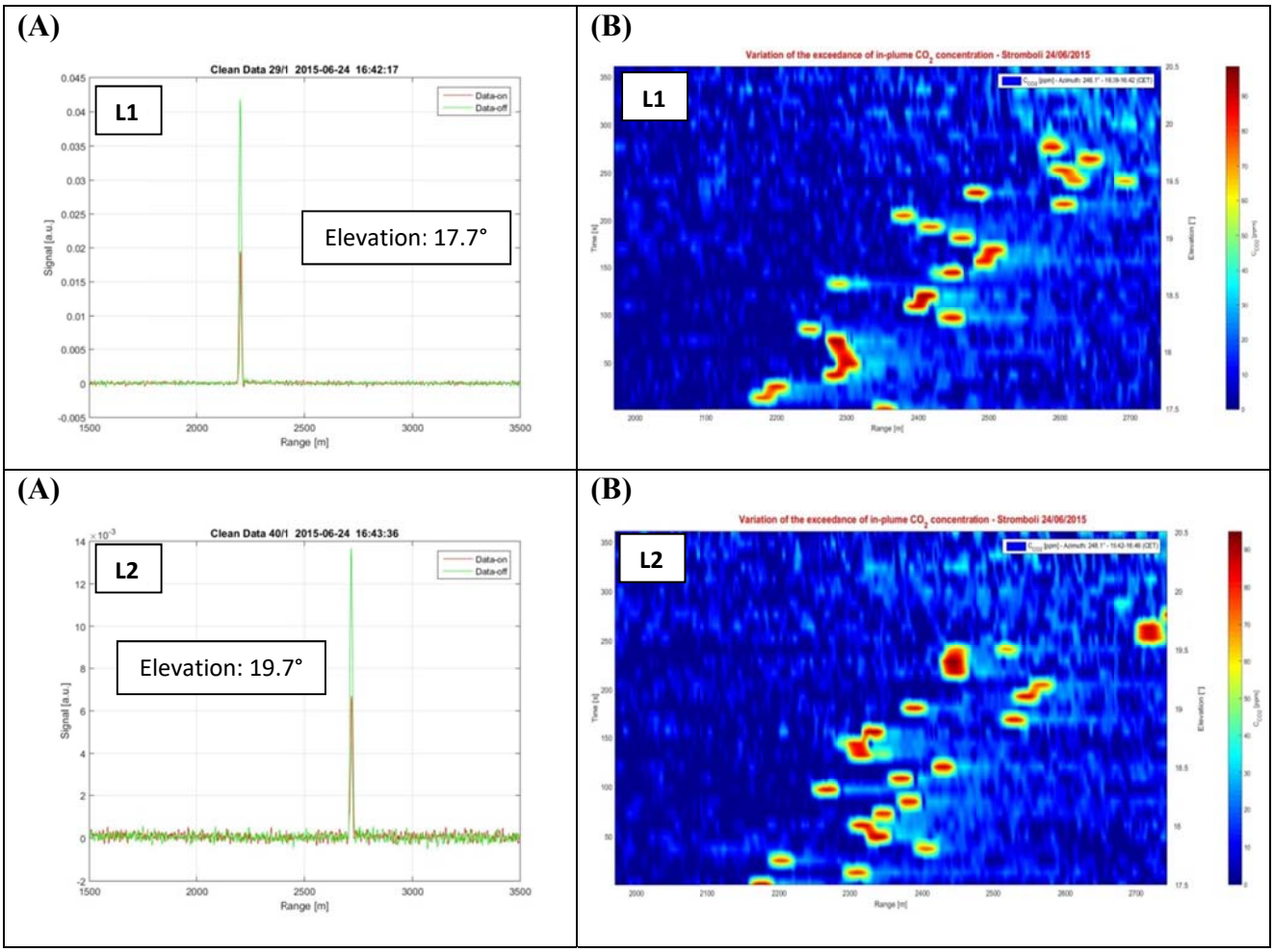

Figure 14) A – *Two example of lidar profile containing CO_2 plume peaks related, respectively, to Loop1 (L1) and 2 (L2) and acquired at different elevation angles.* **B** – *Vertical scans in Cartesian coordinates of the exceedance of in-plume CO_2 concentration as a function of range [m], elevation angle [°] and time [s]. They are related, respectively to Loop1 (L1) and 2 (L2). It is possible to see plume traces from the left to the right side of the map. A reasonable explanation of the high density of CO_2 spots and their movement as a function of time and elevation, could be due to an increase in relative humidity (thus, CO_2 molecules have been condensed into the atmosphere and their scattering properties have been increased), combined with the effect of the wind that have scattered the plume traces from the rockface of Pizzo (left side) to Vancori's peak.*
NB) LOS of the system was pointed on the right side of Pizzo.

"Effetto plume 19-23 verticale"

(A)

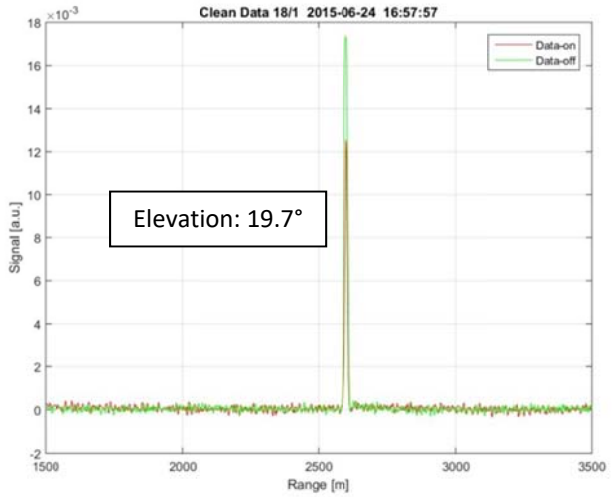

(B)

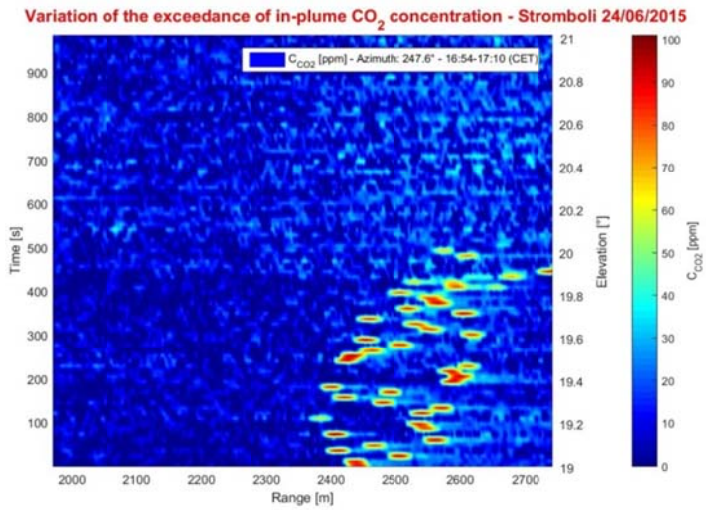

Figure 15)

A – *Example of lidar profile containing CO_2 plume peaks between 2.5 Km and 3 Km.*

B *– Vertical scan in Cartesian coordinates of the exceedance of in-plume CO_2 concentration as a function of range [m], elevation angle [°] and time [s]. It is possible to see plume traces in the bottom right corner of the map. A reasonable explanation of the high density of CO_2 spots could be due to an increase in relative humidity (thus, CO_2 molecules have been condensed into the atmosphere and their scattering properties have been increased), combined with the effect of the wind that have scattered the plume traces next to Vancori's peak.*

NB) LOS of the system was pointed on the right side of Pizzo.

"Scansione Orizzontale"

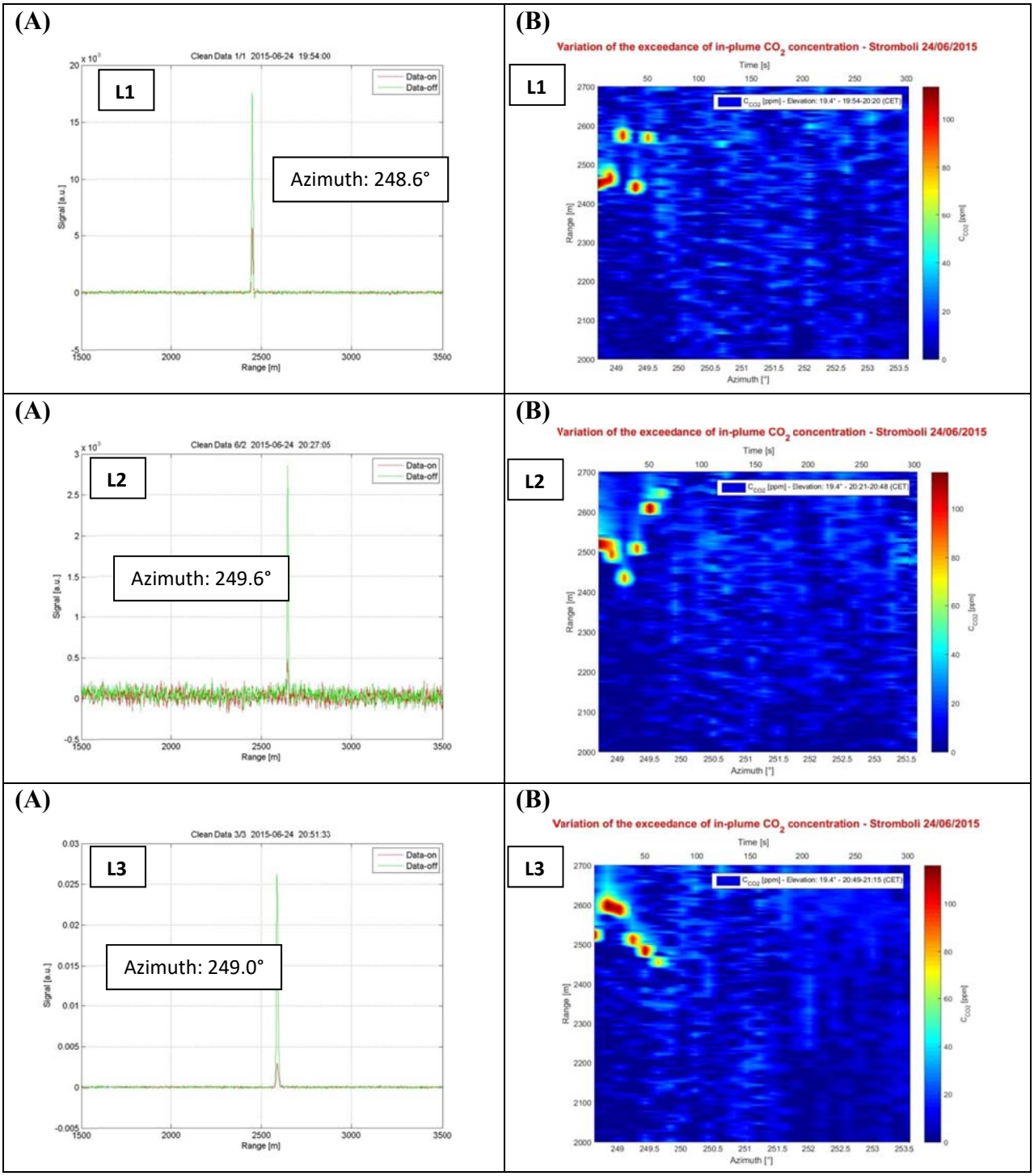

Figure 16) A – *Three example of lidar profile containing CO_2 plume peaks referred, respectively, to Loop1 (L1), 2 (L2) and 3 (L3) and acquired at different azimuth angles.* **B** *– Horizontal scans in Cartesian coordinates of the exceedance of in-plume CO_2 concentration as a function of range [m], azimuth angle [°] and time [s]. They are related, respectively to Loop1 (L1), 2 (L2) and 3 (L3). It is possible to see plume traces at the top left corner of the map. A reasonable explanation of the high density of CO_2 spots and their movement as a function of time and azimuth could be due to an increase in relative humidity (thus, CO_2 molecules have been condensed into the atmosphere and their scattering properties have been increased), combined with the effect of the wind that have scattered the plume traces along the right side of Pizzo's peak. NB) LOS of the system was pointed between the right side of Pizzo and Casuzza.*

4.2 25/06/2015

During the measurement session of the 25 of June, 2015; a significant amount of in-plume CO_2 concentration traces have been detected in two scans. In particular, the attention is focused on:

- "Scansione Orizzontale 2" – horizontal scan, data acquired from 05:43 p.m. to 10:38 p.m. – Figure 18.
- "Scansione Orizzontale 3 notte" – horizontal scan, data acquired from 11:26 p.m. to 09:15 a.m. – Figure 19.

Whereas in "Scansione Orizzontale 1" and also in "Scansione Verticale 2", background noise (with potentially weak plume traces) has been detected.
For further details about the main characteristics of this session, reference is made to Table 7.

"Scansione Orizzontale 2"

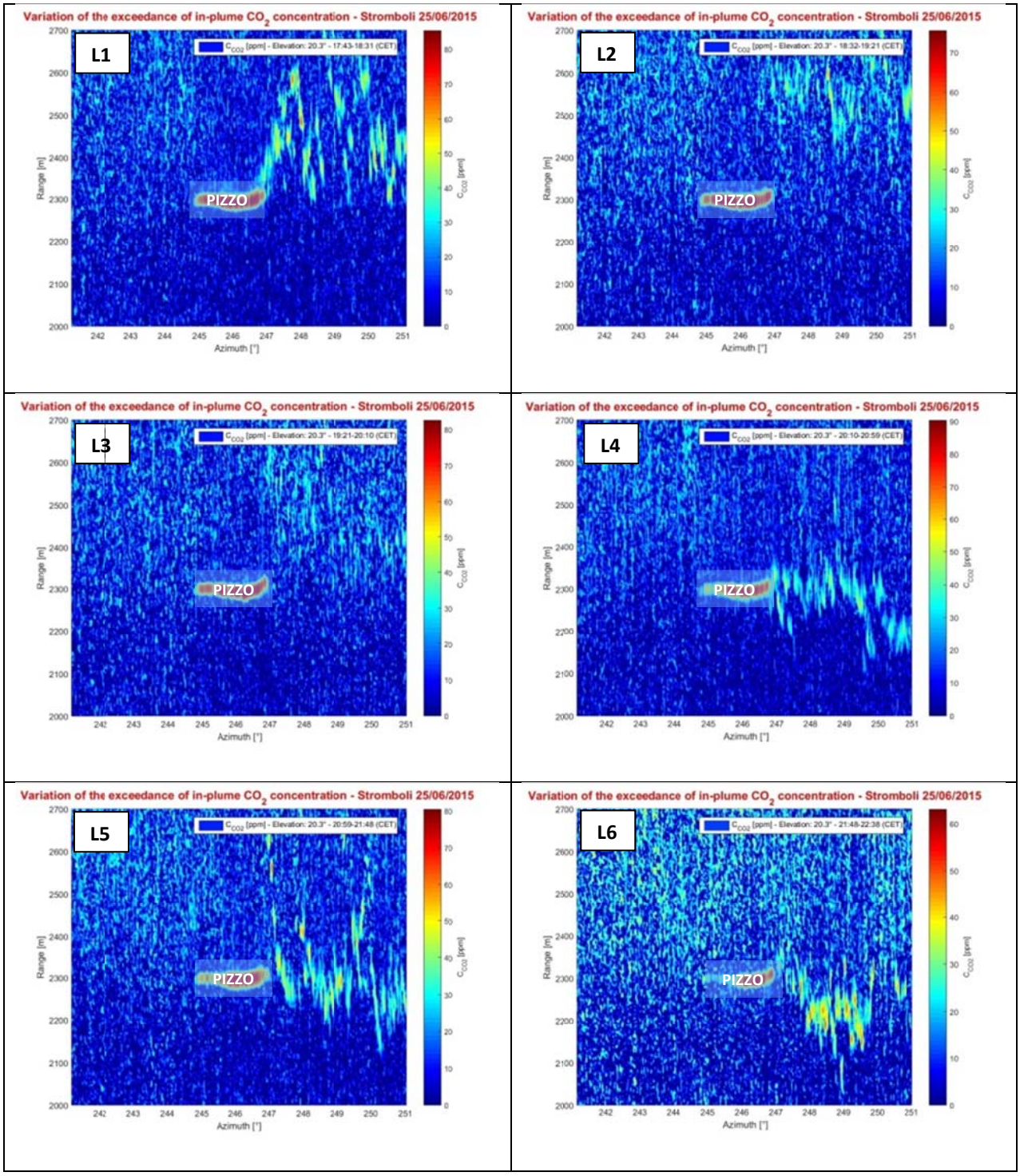

Figure 17) *The six horizontal loops (L1….L6) of the scan have been chronological rearranged so as to show the time evolution of the exceedance of in-plume CO_2 concentration. In the middle of each scan (in Cartesian coordinates) it is possible to see the rockface of Pizzo intercepted by the LOS of the system (azimuth angles: 244.5°-247°, distance of 2300 m from the system), as indicated by the red spot in the middle of each figure. Whereas, on the right side of this orographic obstacle it is clear the variations of CO_2 concentration as a function of time and azimuth angles. A reasonable explanation of this fact could be due to the effect of the wind that have scattered the plume traces from Pizzo to Casuzza.*
NB) LOS of the system was pointed between the right side of Vancori and Casuzza.

“Scansione Orizzontale 3 notte”

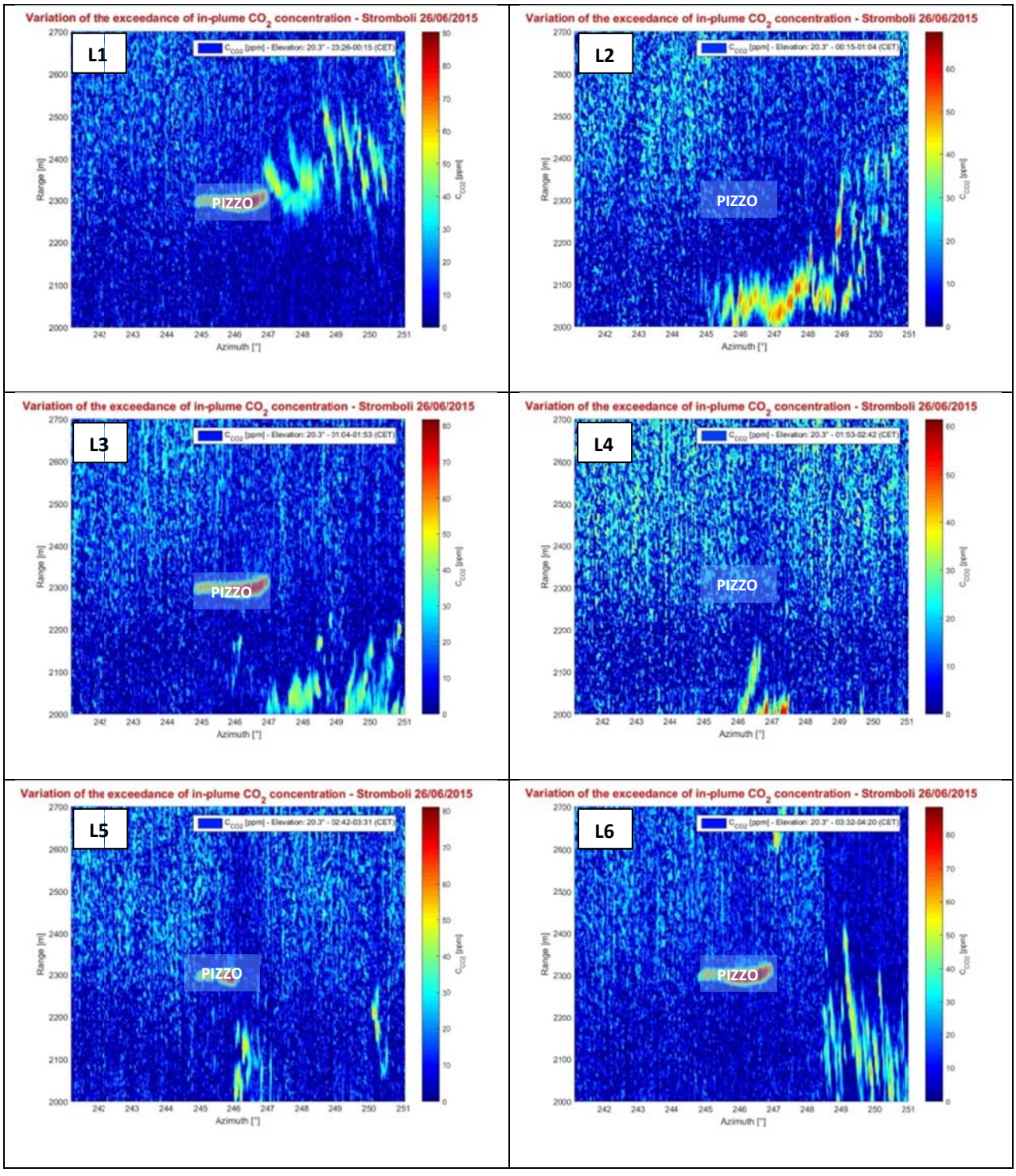

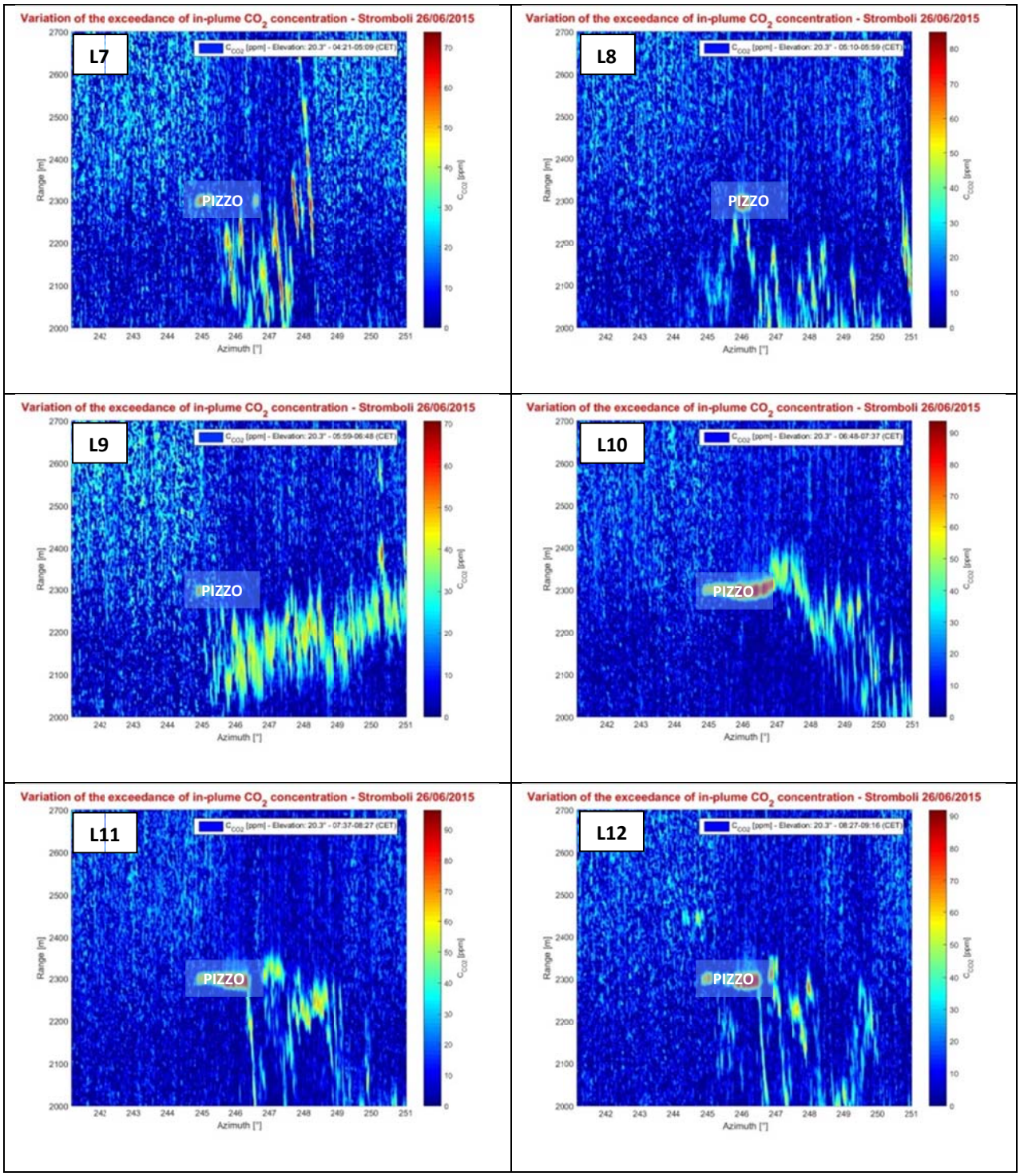

Figure 18) *The twelve horizontal loops (L1….L12) of the scan have been chronological rearranged so as to show the time evolution of the exceedance of in-plume CO_2 concentration. In the middle of each scan (in Cartesian coordinates) it is possible to see the rockface of Pizzo intercepted by the LOS of the system (azimuth angles: 244.5°-247°, distance of 2300 m from the system), as indicated by the red spot in the middle of each figure. Whereas, on the right side of this orographic obstacle it is clear the variations of CO_2 concentration as a function of time and azimuth. It is important to note that in some maps the rockface of Pizzo is not visible, partially or entirely covered by the plume (located in the bottom side of the figure in these particular cases). This is particularly true during the nighttime session and could be probably due to the increase in relative humidity (therefore, CO_2 molecules have been condensed into the atmosphere and their scattering properties have been increased), combined with the effect of the wind that have scattered the plume traces along the right side of Pizzo's peak. NB) LOS of the system was pointed between the right side of Vancori and Casuzza.*

4.3 <u>26/06/2015</u>

During the measurement session of the 26 of June, 2015; a significant amount of in-plume CO_2 concentration traces have been detected in several scans. In particular, the attention is focused on:

- "Scansione Orizzontale dopo la calibrazione della cella" – horizontal scan, data acquired from 10:21 a.m. to 10:52 a.m. – Figure 20.
- "Scansione Verticale 1 Vancori" – vertical scan, data acquired from 10:57 a.m. to 11:20 a.m. – Figure 21.
- "Scansione Verticale 2 Vancori 4loop" – vertical scan, data acquired from 11:26 a.m. to 00:45 p.m. – Figure 22.
- "Scansione Verticale 7 notte" – vertical scan, data acquired from 00:17 a.m. to 02:41 a.m. – Figure 24.

Except for "Scansione Verticale 4", in which the rockface of Pizzo next to Casuzza has been detected (this fact is true only for even lidar signals), other scans showed only the background noise. On this regard, see Figure 23.
For further details about the main characteristics of this session, reference is made to Table 7.

"Scansione Orizzontale dopo la calibrazione della cella"

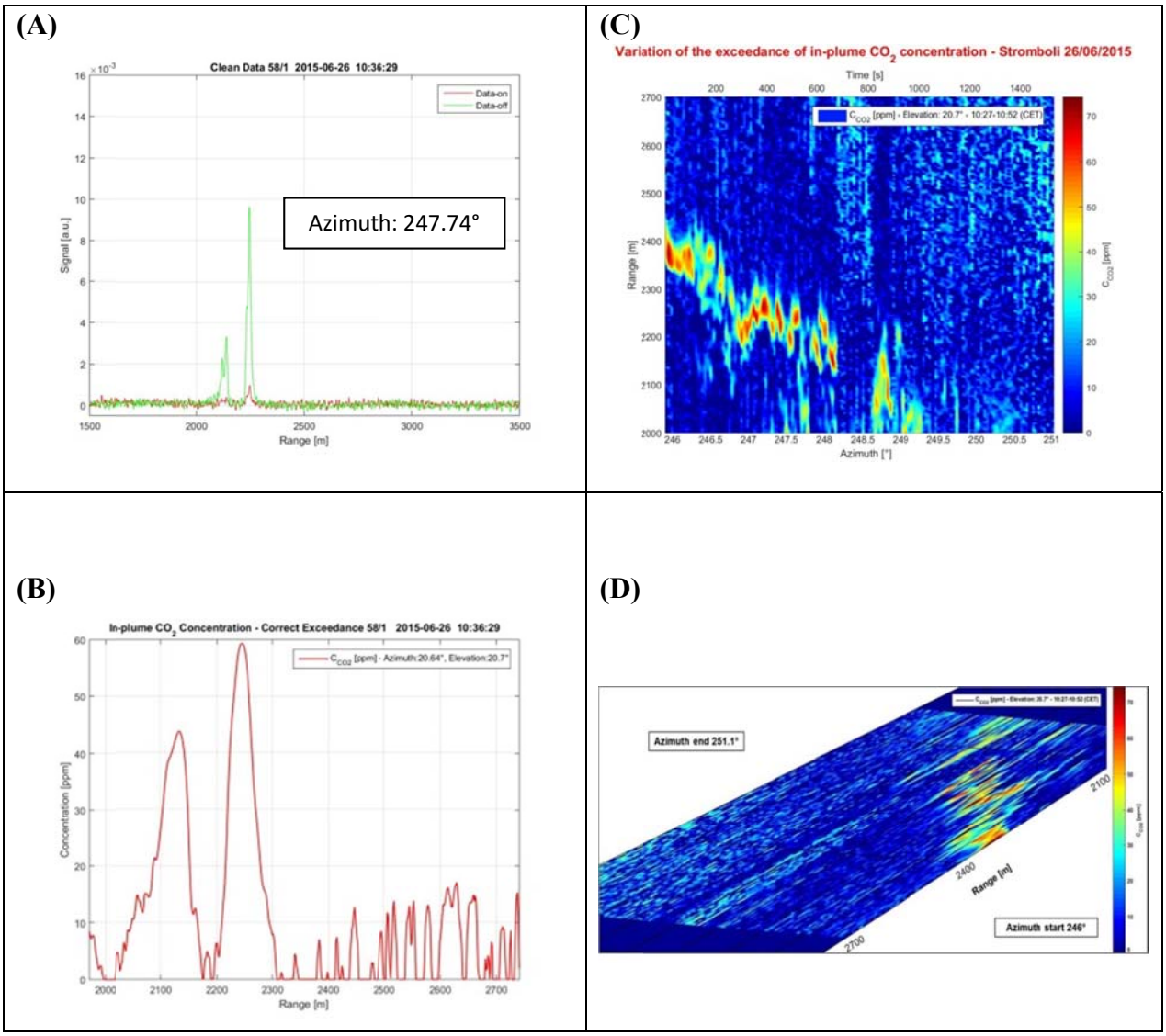

Figure 19) A – *Example of lidar profile containing CO_2 plume peaks between 2 Km and 2.5 Km.* **B** *– In-plume CO_2 concentration profile related to Figure 20 -* ***A****. Horizontal scan in Cartesian -* **C** *and polar coordinates -* **D** *of the exceedance of in-plume CO_2 concentration as a function of range [m], azimuth angle [°] and time [s]. It is possible to see plume traces from the left side to the bottom middle of the map. A reasonable explanation of the dispersion of CO_2 spots (as a function of azimuth angle and the time) could be due to the effect of the wind that have scattered the plume traces from the rockface of Pizzo to Casuzza.*
NB) LOS of the system was pointed between the right side of Pizzo and Casuzza.

"Scansione Verticale 1 Vancori"

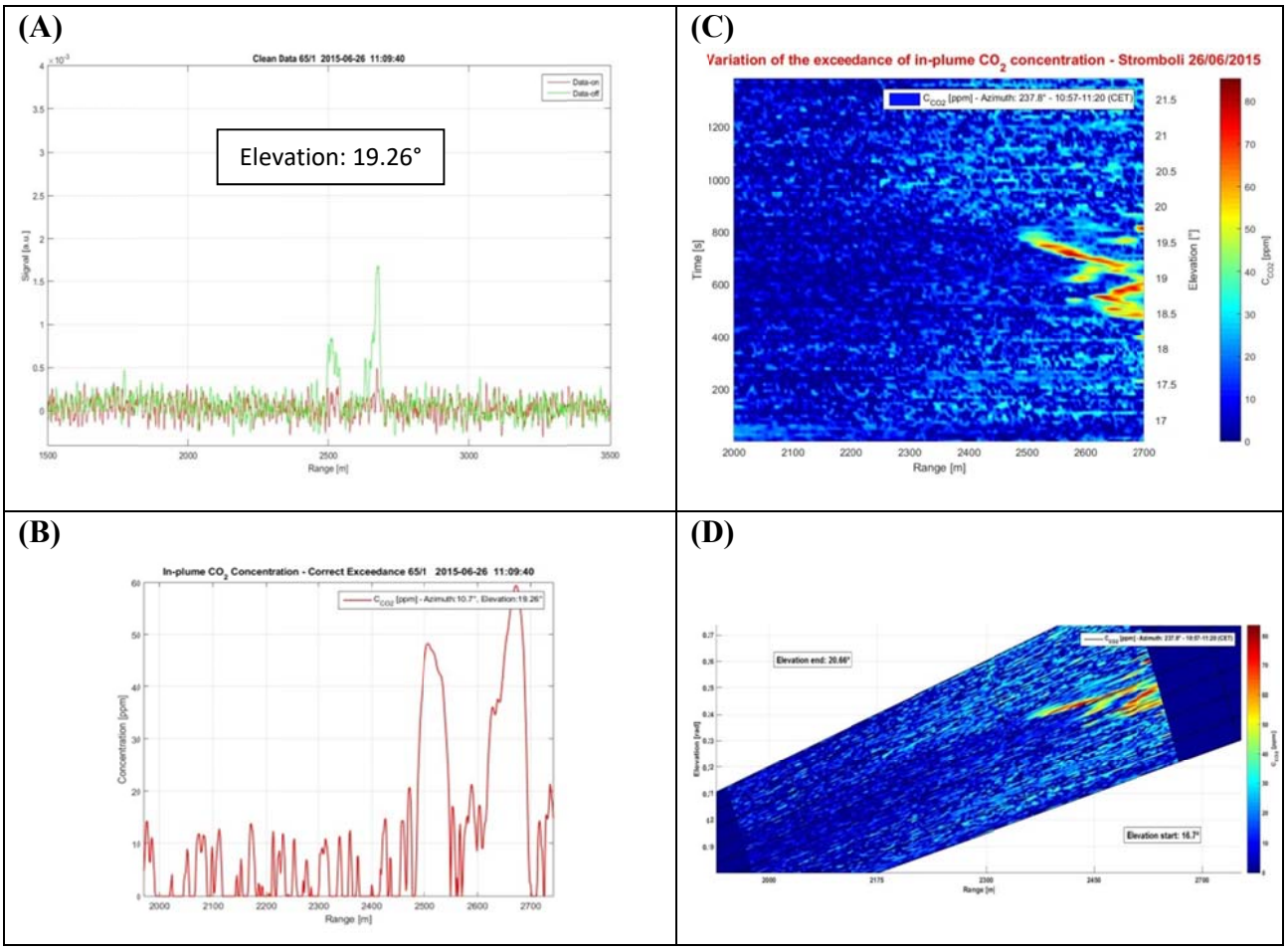

Figure 20) A – *Example of lidar profile containing CO_2 plume peaks between 2.5 Km and 3 Km.* **B** *– In-plume CO_2 concentration profile related to Figure 21 -* ***A****. Vertical scan in Cartesian -* **C** *and polar coordinates -* **D** *of the exceedance of in-plume CO_2 concentration as a function of range [m], elevation angle [°] and time [s]. It is possible to see a time-resolved plume evolutiom on the right side of the map. A reasonable explanation of the dispersion of CO_2 spots (as a function of elevation angle and the time) could be due to the effect of the wind that have scattered the plume traces next to Vancori's peak.*
NB) LOS of the system was pointed to Vancori (rockface).

“Scansione Verticale 2 Vancori 4loop”

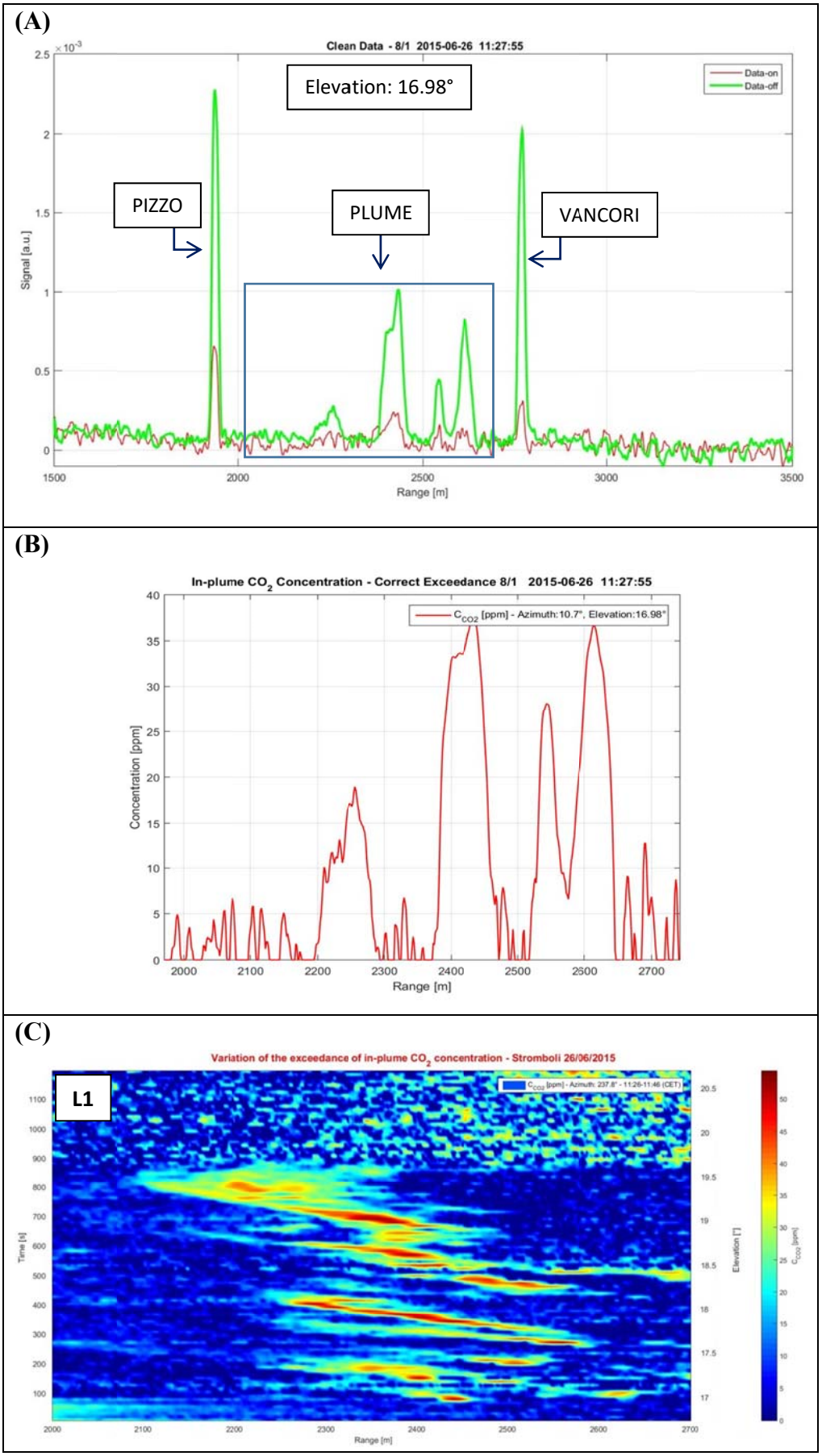

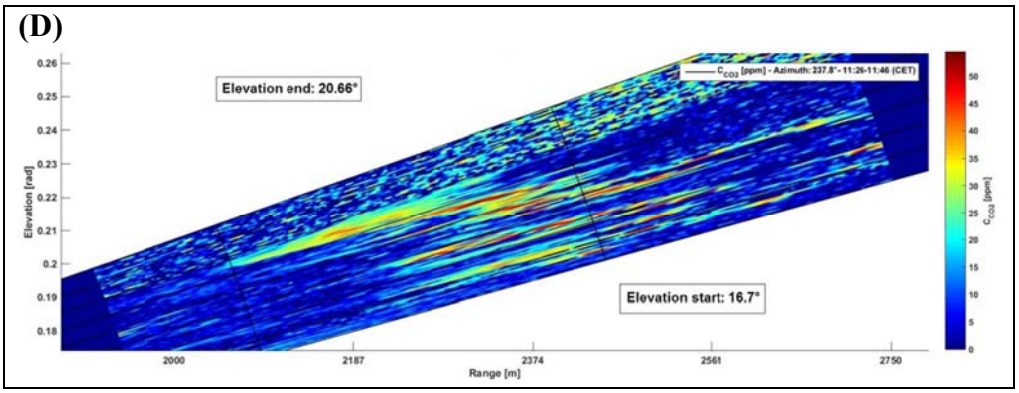

Figure 21) A – *Example of lidar profile containing CO_2 plume peaks between 2 Km and 2.7 Km.* **B** *– In-plume CO_2 concentration profile related to Figure 22 -* **A** *. Vertical scan in Cartesian -* **C** *and polar coordinates -* **D** *of the exceedance of in-plume CO_2 concentration as a function of range [m], elevation angle [°] and time [s]. It is possible to see a complete time-resolved plume evolution in the middle of the map. A reasonable explanation of the dispersion of CO_2 spots (as a function of elevation angle and the time) could be due to the effect of the wind that have scattered these plume traces up in the atmosphere.*
NB) LOS of the system was pointed to Vancori (rockface).

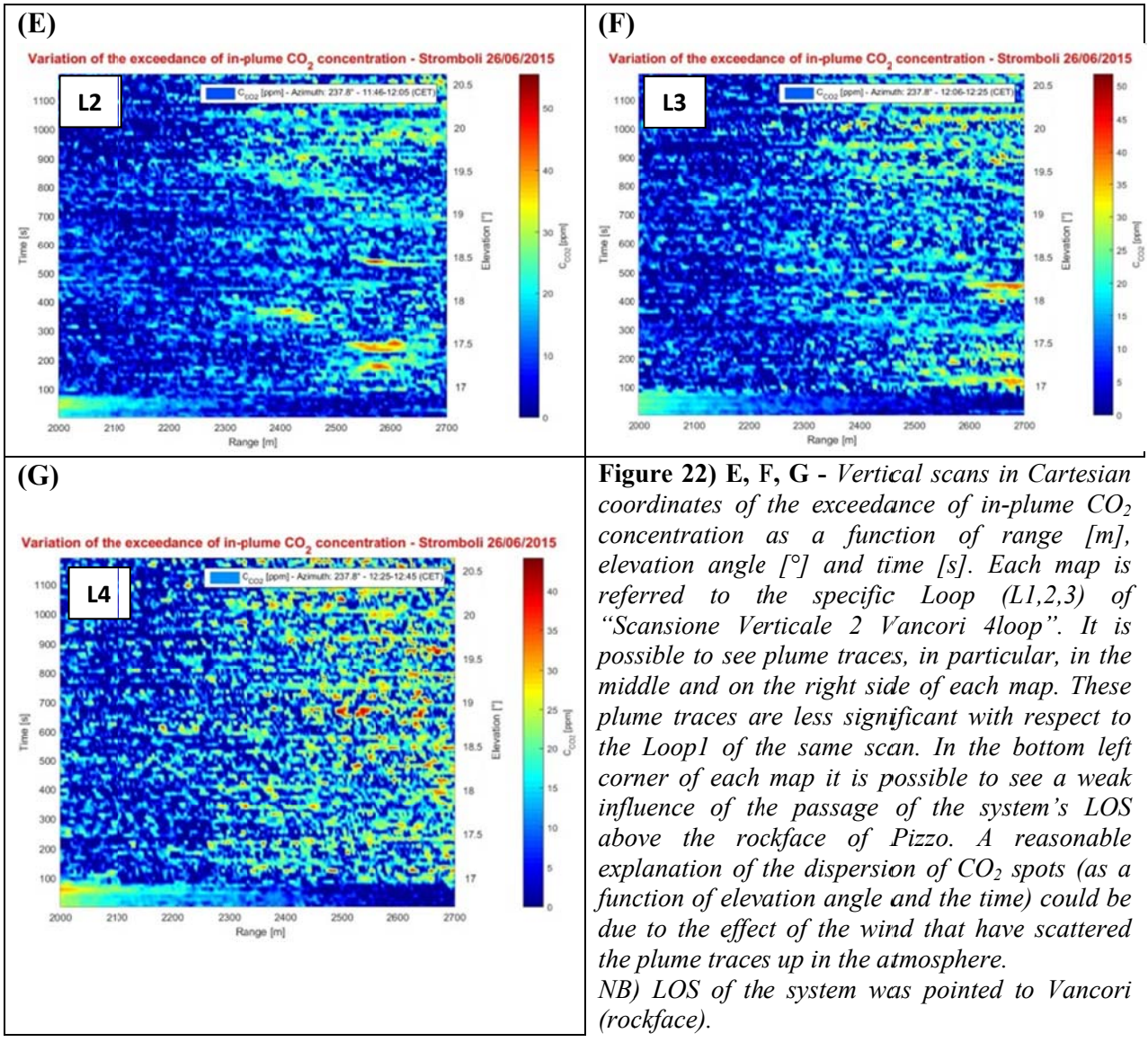

Figure 22) E, F, G - *Vertical scans in Cartesian coordinates of the exceedance of in-plume CO_2 concentration as a function of range [m], elevation angle [°] and time [s]. Each map is referred to the specific Loop (L1,2,3) of "Scansione Verticale 2 Vancori 4loop". It is possible to see plume traces, in particular, in the middle and on the right side of each map. These plume traces are less significant with respect to the Loop1 of the same scan. In the bottom left corner of each map it is possible to see a weak influence of the passage of the system's LOS above the rockface of Pizzo. A reasonable explanation of the dispersion of CO_2 spots (as a function of elevation angle and the time) could be due to the effect of the wind that have scattered the plume traces up in the atmosphere.*
NB) LOS of the system was pointed to Vancori (rockface).

"Scansione Verticale 4"

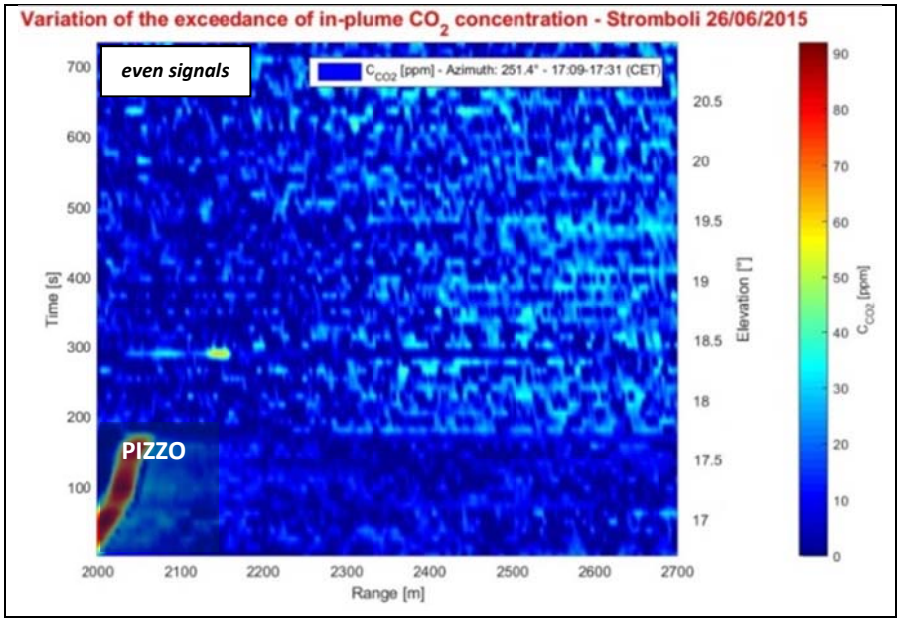

Figure 23) *Vertical scan in Cartesian coordinates of the exceedance of in-plume CO_2 concentration as a function of range [m], elevation angle [°] and time [s]. It is possible to see the rockface of Pizzo next to Casuzza, intercepted by the LOS of the system (elevation angles: 16.7°-21.02°), as indicated by the red spot in the bottom left corner of the map. Above this orographic obstacle is also visible a weak trace of plume.*
Note that this map regards only even lidar signals. Whereas in the map concerning odd signals it has been detected only the background noise.
NB) LOS of the system was pointed to Casuzza (on the right side of Pizzo rockface).

"Scansione Verticale 7 notte"

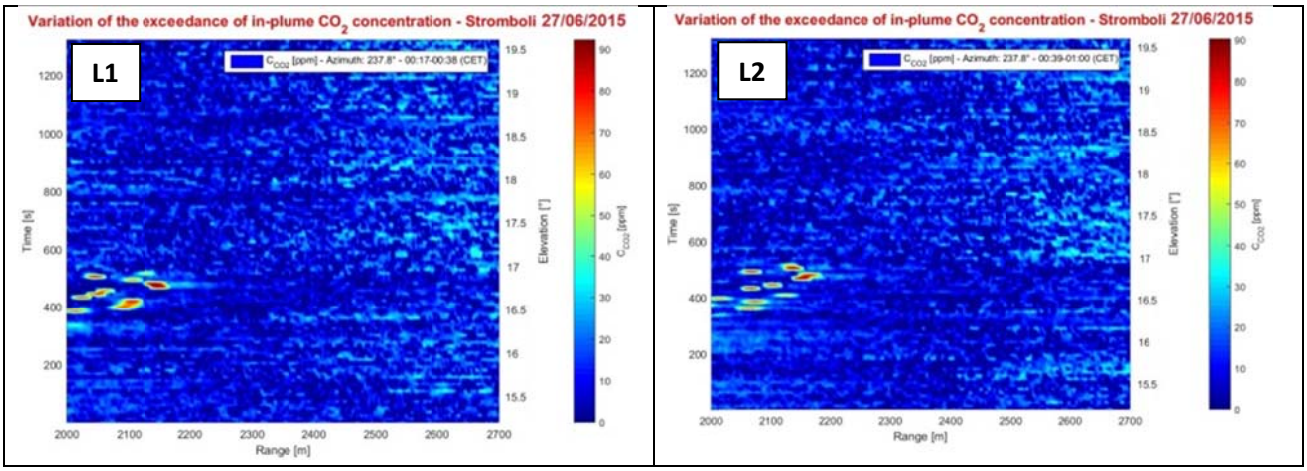

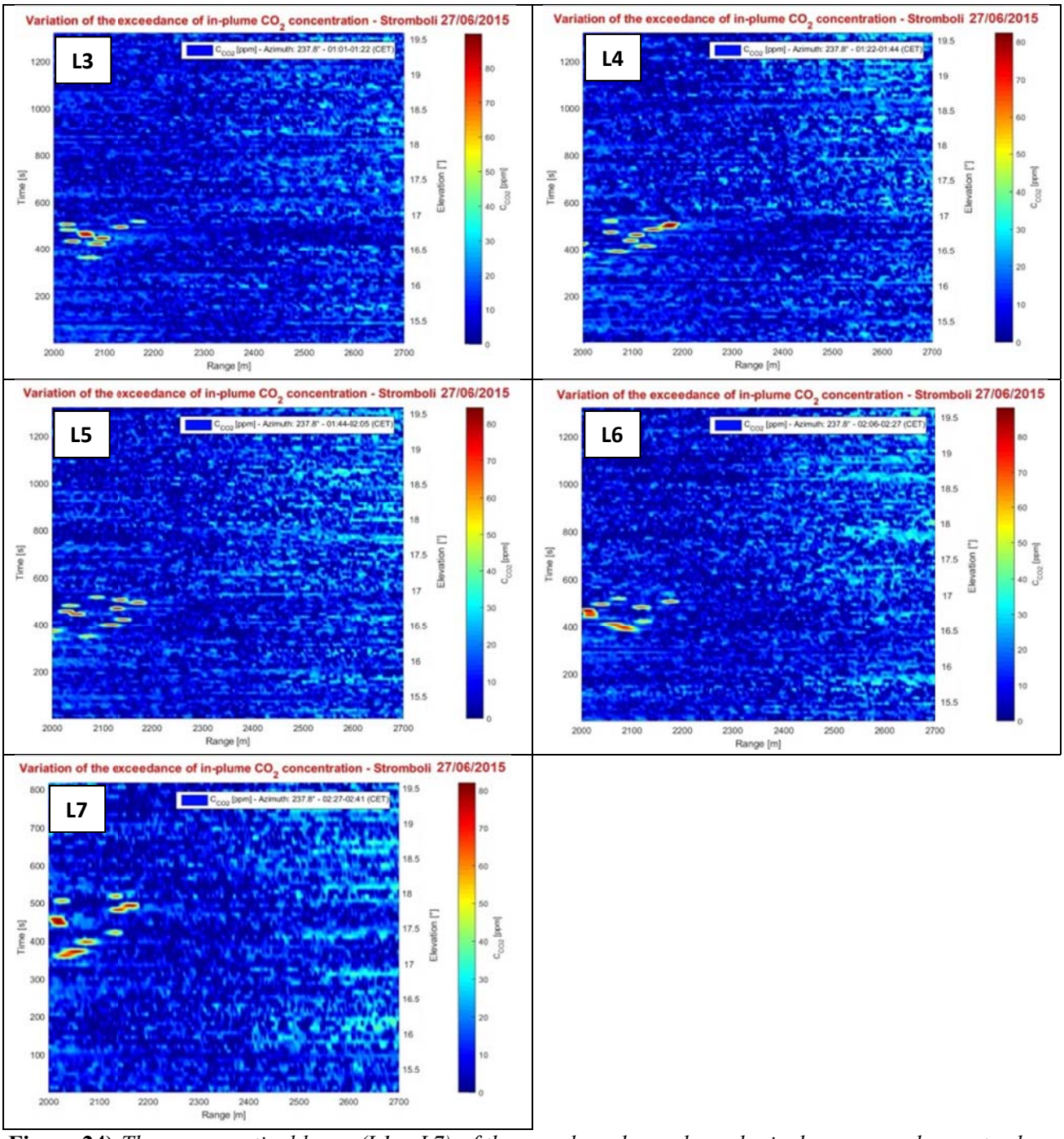

Figure 24) *The seven vertical loops (L1….L7) of the scan have been chronological rearranged so as to show the time evolution of the exceedance of in-plume CO_2 concentration. On the left side of each scan (in Cartesian coordinates) it is possible to see the variations of CO_2 concentration as a function of time and elevation. It is important to note that plume traces are extremely dense and continuously change their position. As already shown in Figures 18 and 19, this fact is particularly true during the nighttime session and could be probably due to the increase in relative humidity (therefore, CO_2 molecules have been condensed into the atmosphere and their scattering properties have been increased), combined with the effect of the wind that have scattered the plume traces above the rockface of Pizzo.*
NB) LOS of the system was pointed to Vancori (rockface).

As already mentioned, during the experimental campaign the detection of plume traces after the position of Vancori's peak (farther than 3 Km) was extremely rare. Nonetheless, in the following Figures (25 – A, B), related to Loop1 of "Scansione Verticale 7 notte", there are some significant examples of this type.
Moreover, in Figure 25 – C is reported the vertical scan in Cartesian coordinates of the exceedance of in-plume CO_2 concentration as a function of range [m], elevation angle [°] and time [s]. The essential feature of this scan, related to Loop1, is the extension of range between 2 Km and 3.5 Km. In fact, some CO_2 plume traces are clearly visible beyond 3 Km and for elevation angles greater than the threshold of Vancori's peak.

(A) 26/06/2015 – "Scansione Verticale 7 notte" – Loop1/Signal64. El:17.72° - Az:237.8°

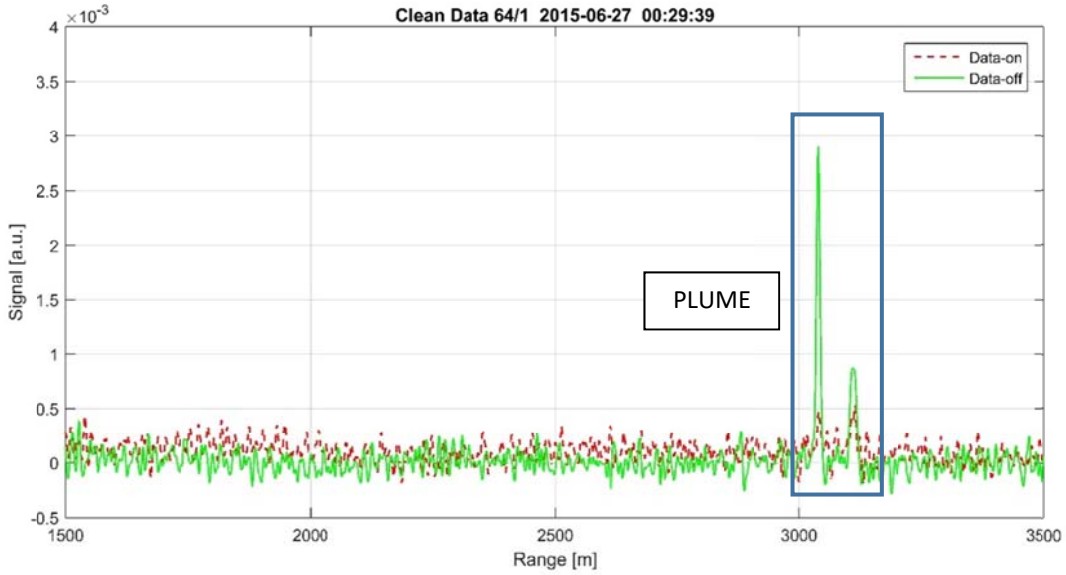

(B) 26/06/2015 – "Scansione Verticale 7 notte" – Loop1/Signal65. El:17.76° - Az:237.8°

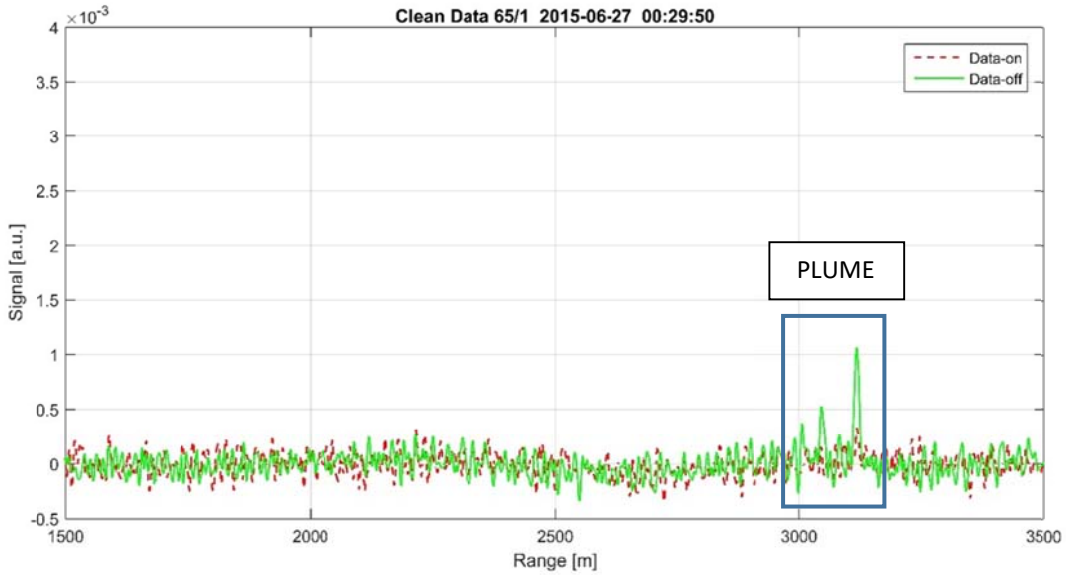

(C) 26/06/2015 – "Scansione Verticale 7 notte" – Loop1.

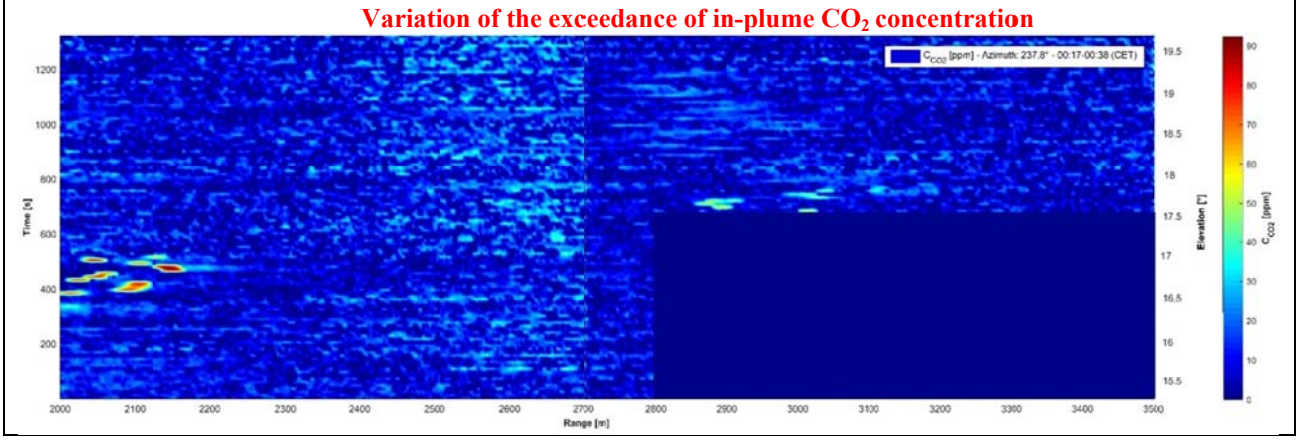

Figure 25) A – *Example of Lidar profile n°64, Loop1, "Scansione Verticale 7 notte", Elevation angle: 17.72°, Azimuth angle: 237.8°. It is possible to see a double CO_2 in-plume peak between 3 Km and 3.2 Km.* **B** – *Example of Lidar profile n°65, Loop1, "Scansione Verticale 7 notte", Elevation angle: 17.76°, Azimuth angle: 237.8°. It is possible to see a triple CO_2 in-plume peak between 3 Km and 3.2 Km.* **C** - *Vertical scan in Cartesian coordinates of the exceedance of in-plume CO_2 concentration related to Loop1 of "Scansione verticale 7 notte" as a function of range [m], elevation angle [°] and time [s]. It is possible to see some traces of in-plume CO_2 concentration on the left and beyond 2.9 Km, for elevation angles greater than the threshold of Vancori's peak. As already stressed in Figure 24, the high density of CO_2 plume traces could be probably due to the increase in relative humidity during the nighttime session. This phenomenon, combined with the effect of the wind, has probably scattered the plume traces from the side of Pizzo above the Vancori's peak.*
Note that the dark blue portion indicate an interval without measurements.
NB) LOS of the system was pointed to Vancori (rockface).

4.4 <u>27/06/2015</u>

During the measurement session of the 27 of June, 2015; the background noise with weak plume traces has been detected in every scan.
For this reason, the dispersion maps of in-plume CO_2 concentration aren't shown in this report.
For further details about the main characteristics of this session, reference is made to Table 7.

4.5 <u>28/06/2015</u>

During the measurement session of the 28 of June, 2015; a significant amount of in-plume CO_2 concentration traces have been detected in several scans. In particular, the attention is focused on:

- "Scansione Verticale 4" – vertical scan, data acquired from 05:18 p.m. to 06:12 p.m. – Figure 26.
- "Scansione Verticale 5" – vertical scan, data acquired from 06:49 p.m. to 11:49 p.m. – Figure 27 (first part).

Instead, in other scans the background noise has been detected.
For further details about the main characteristics of this session, reference is made to Table 7.

"Scansione Verticale 4"

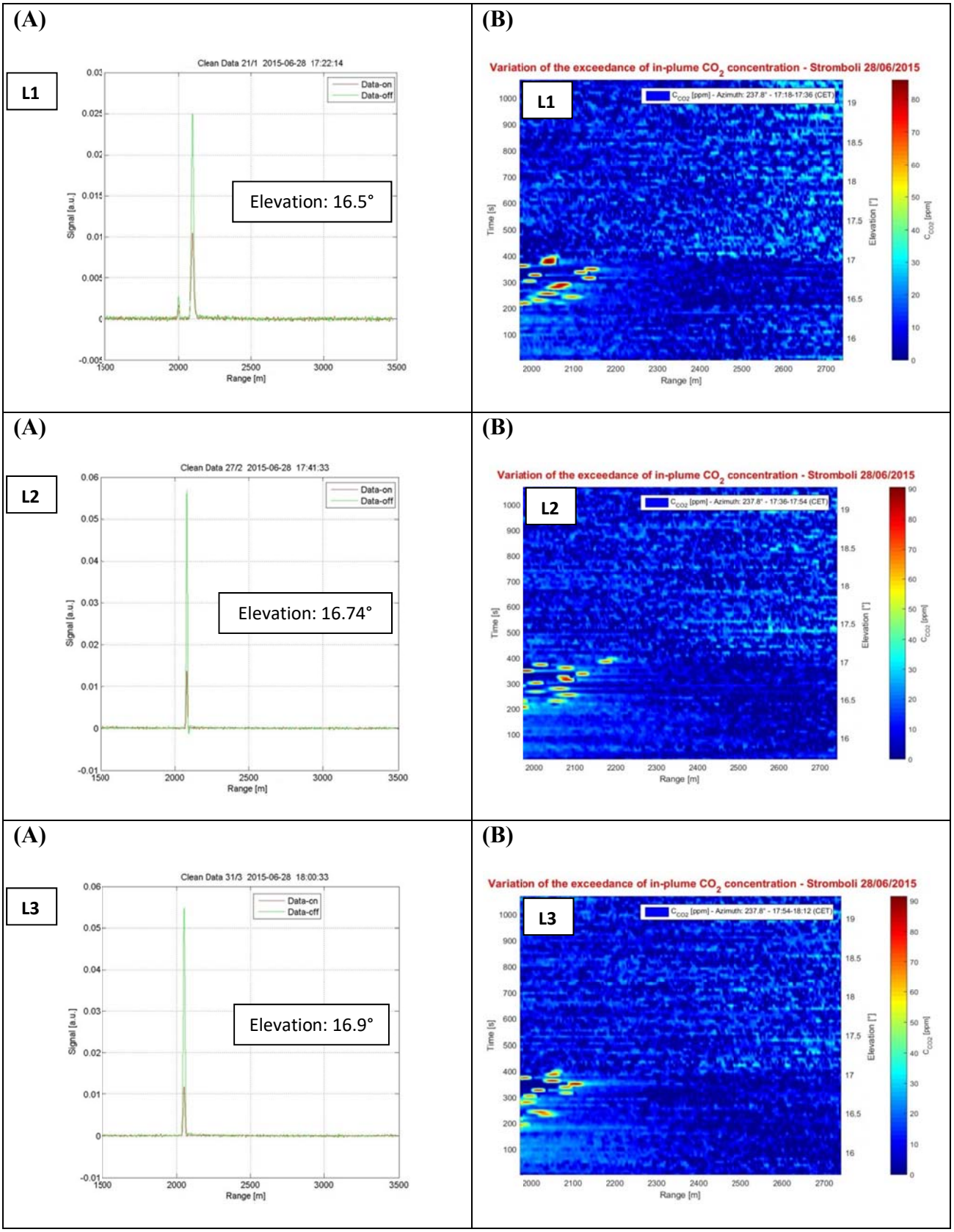

Figure 26) A – *Three example of lidar profile containing CO_2 plume peaks referred, respectively, to Loop1 (L1), 2 (L2) and 3 (L3) and acquired at different elevation angles.* **B** *– The three loops of the scan have been chronological rearranged so as to show the time evolution of the exceedance of in-plume CO_2 concentration. These vertical scans, expressed in Cartesian coordinates as a function of range [m], elevation angle [°] and*

time [s], are related, respectively, to Loop1 (L1), 2 (L2) and 3 (L3). It is possible to see plume traces in the bottom left corner of the map. A reasonable explanation of the high density of CO_2 spots and their movement as a function of time and elevation could be due to an increase in relative humidity (thus, CO_2 molecules have been condensed into the atmosphere and their scattering properties have been increased), combined with the effect of the wind that have scattered the plume traces above the rockface of Pizzo.
NB) LOS of the system was pointed to Vancori (rockface).

"Scansione Verticale 5" (1-17 Loop)

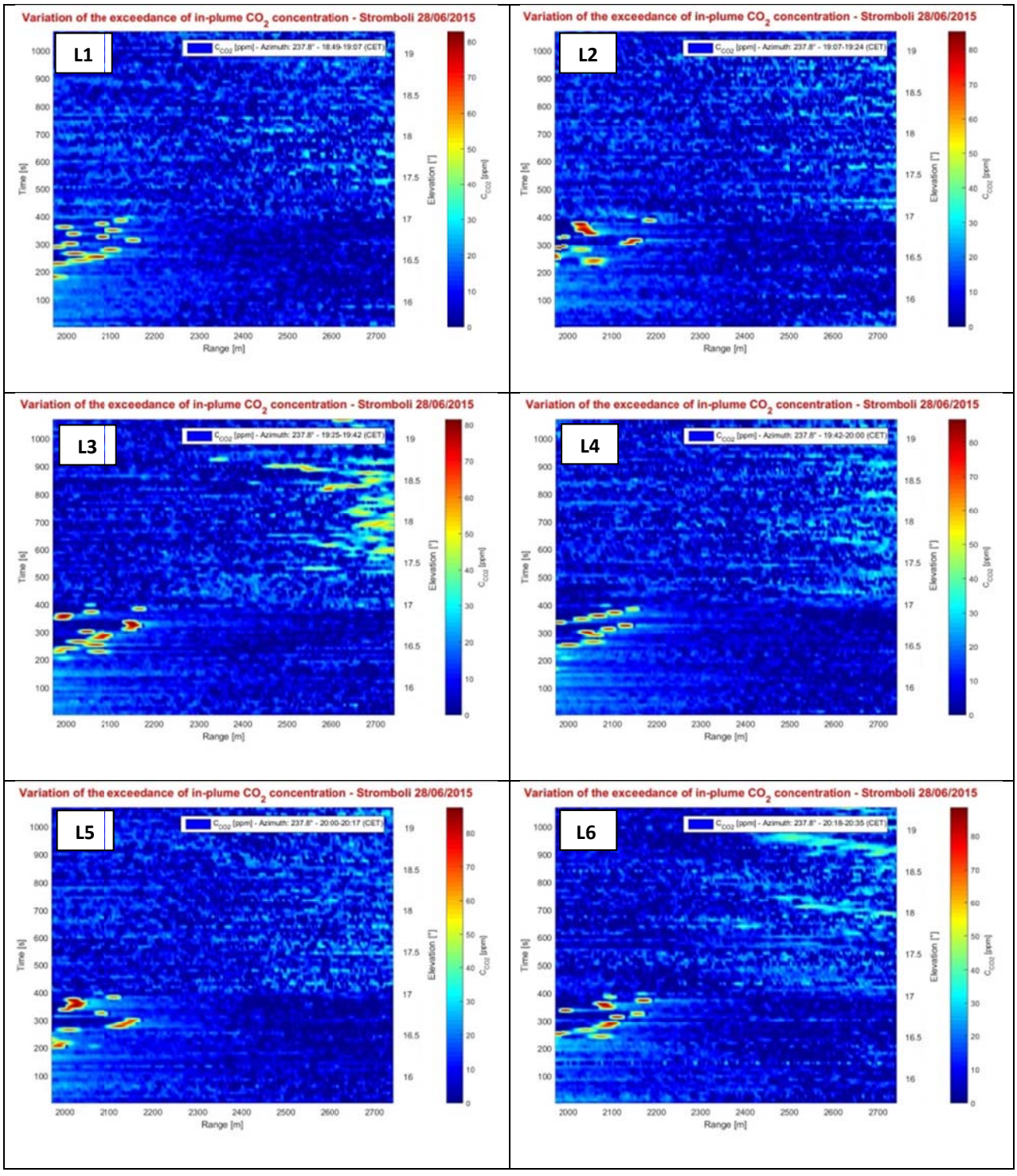

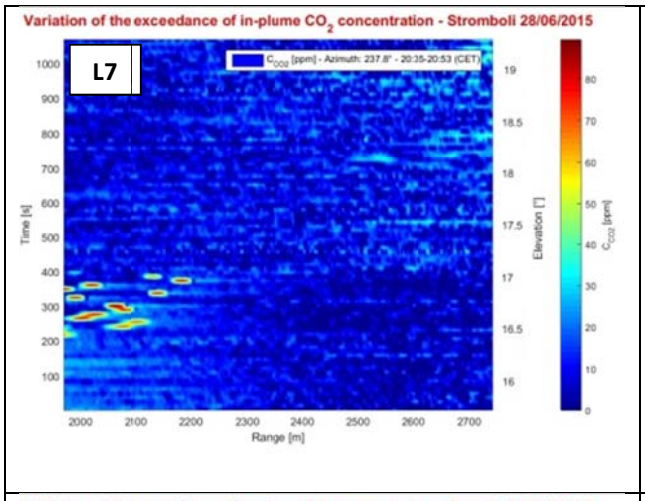
Variation of the exceedance of in-plume CO_2 concentration - Stromboli 28/06/2015
L7
Time [s]
Range [m]
Elevation [°]
C_{CO2} [ppm]

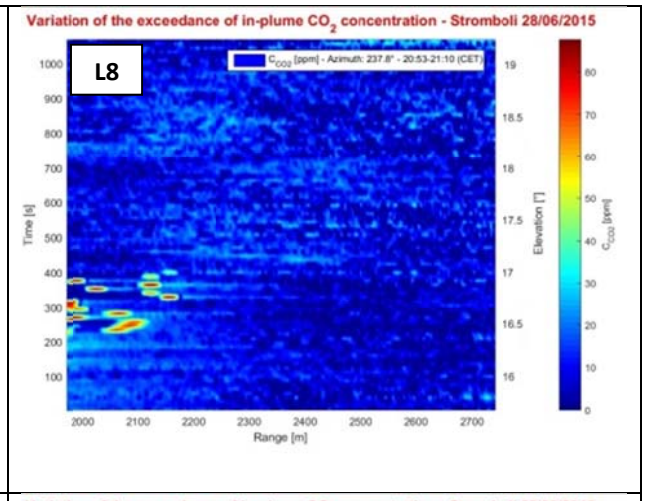
Variation of the exceedance of in-plume CO_2 concentration - Stromboli 28/06/2015
L8
Time [s]
Range [m]
Elevation [°]
C_{CO2} [ppm]

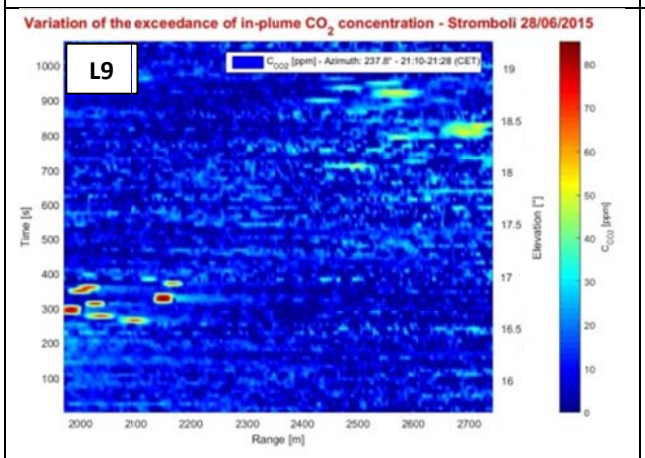
Variation of the exceedance of in-plume CO_2 concentration - Stromboli 28/06/2015
L9
Time [s]
Range [m]
Elevation [°]
C_{CO2} [ppm]

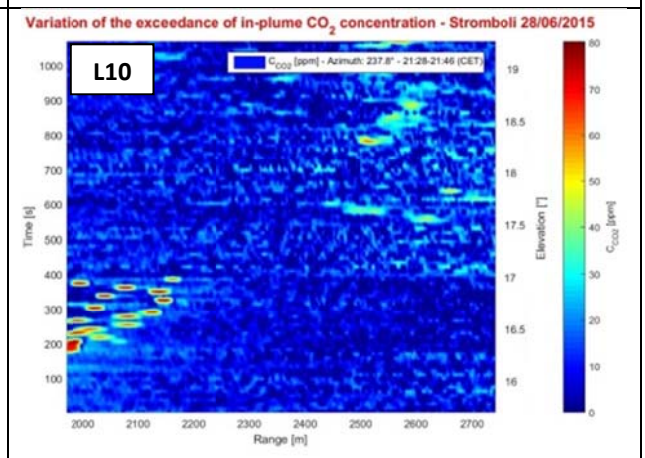
Variation of the exceedance of in-plume CO_2 concentration - Stromboli 28/06/2015
L10
Time [s]
Range [m]
Elevation [°]
C_{CO2} [ppm]

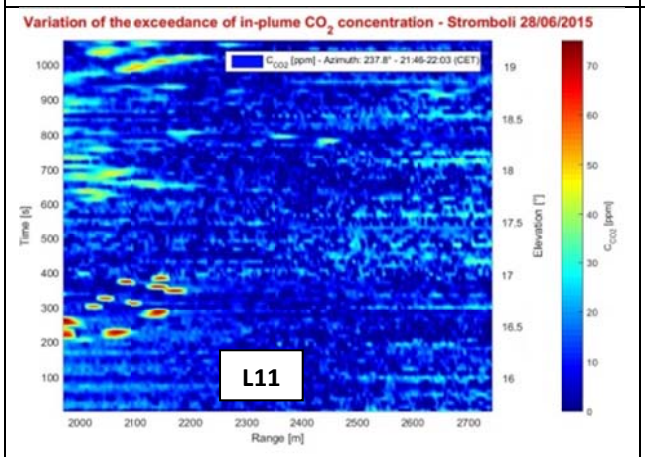
Variation of the exceedance of in-plume CO_2 concentration - Stromboli 28/06/2015
L11
Time [s]
Range [m]
Elevation [°]
C_{CO2} [ppm]

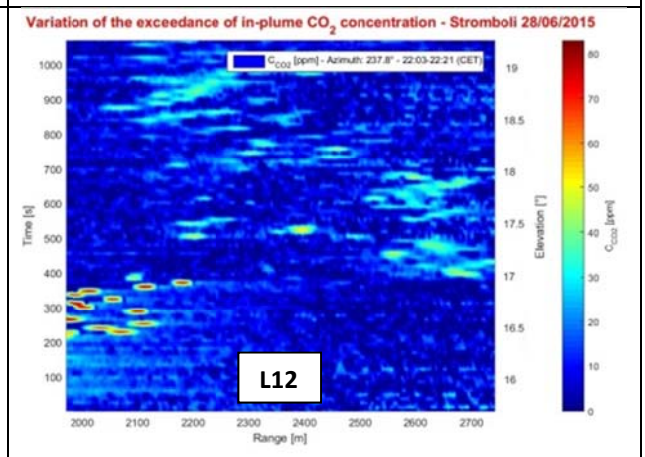
Variation of the exceedance of in-plume CO_2 concentration - Stromboli 28/06/2015
L12
Time [s]
Range [m]
Elevation [°]
C_{CO2} [ppm]

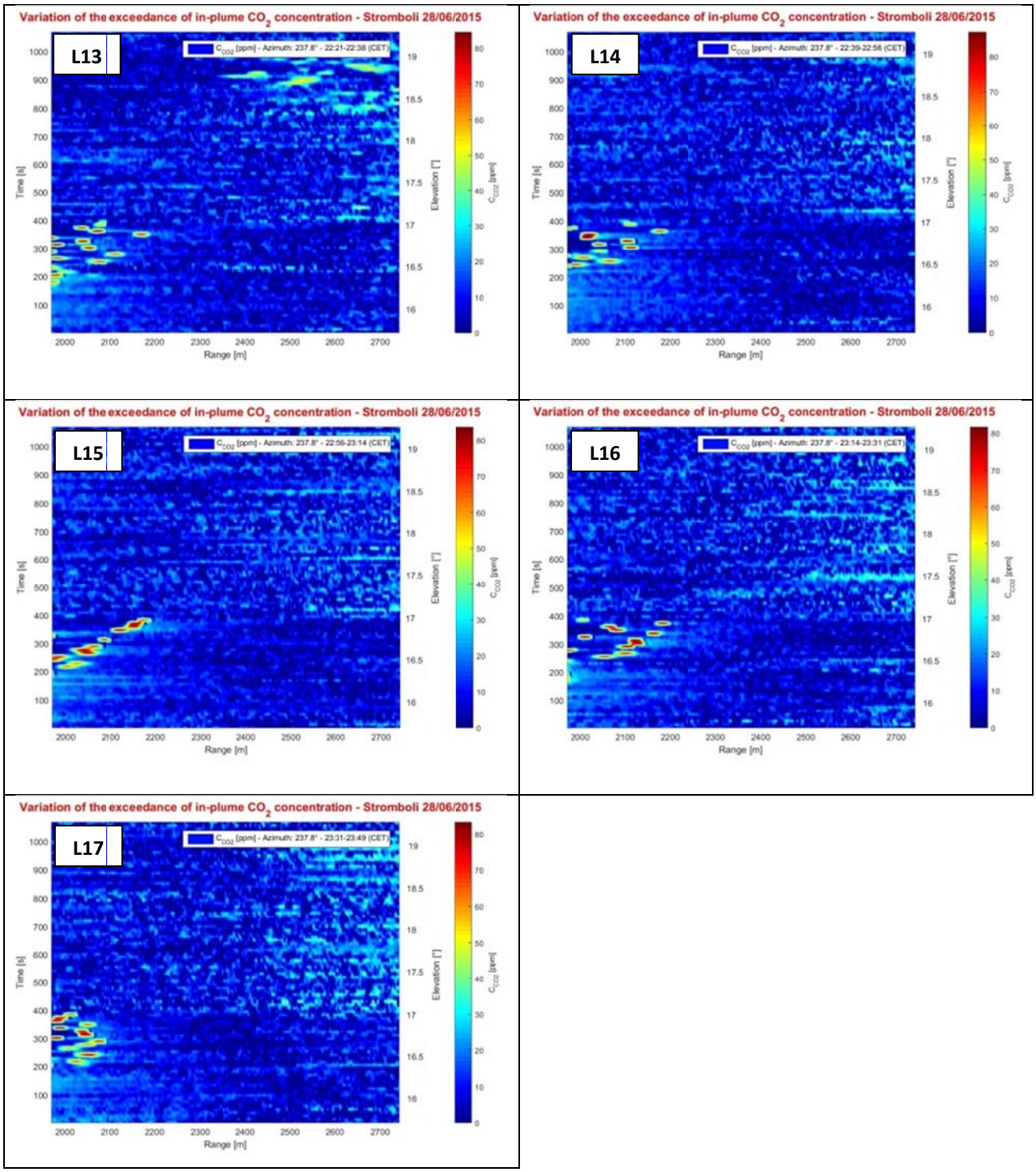

Figure 27) *The seventeen vertical loops (L1….L17) of the scan have been chronological rearranged so as to show the time evolution of the exceedance of in-plume CO_2 concentration. In the bottom left corner and on the upper ride side of each scan (in Cartesian coordinates) it is possible to see the variations of CO_2 concentration as a function of time and elevation. It is important to note that plume traces in the bottom left corner are extremely dense and continuously change their position; instead plume traces on the upper right side are less dense but more spread than the previous ones. As already shown in Figures 18 and 24 this fact is particularly true during the nighttime session and could be probably due to the increase in relative humidity (therefore, CO_2 molecules have been condensed into the atmosphere and their scattering properties have been increased), combined with the effect of the wind that have scattered the plume traces above the rockface of Pizzo and then up in the atmosphere.*
NB) LOS of the system was pointed to Vancori (rockface).

As already shown in Section 4.3, also during the measurement session of the 28 of June, some plume traces have been detected after the position of Vancori's peak (farther than 3 Km). In the following Figures (28 – A, B), related to Loop6 of "Scansione Verticale 5", there are some significant examples of this type.
Moreover, in Figure 28 – C is reported the vertical scan in Cartesian coordinates of the exceedance of in-plume CO_2 concentration as a function of range [m], elevation angle [°] and time [s]. The essential feature of this scan, related to Loop6, is the extension of range between 2 Km and 3.5 Km. In fact, some CO_2 plume traces are clearly visible beyond 3 Km and for elevation angles greater than the threshold of Vancori's peak.

(A) 28/06/2015 – "Scansione Verticale 5" – Loop6/Signal53. El:17.78° - Az:237.8°

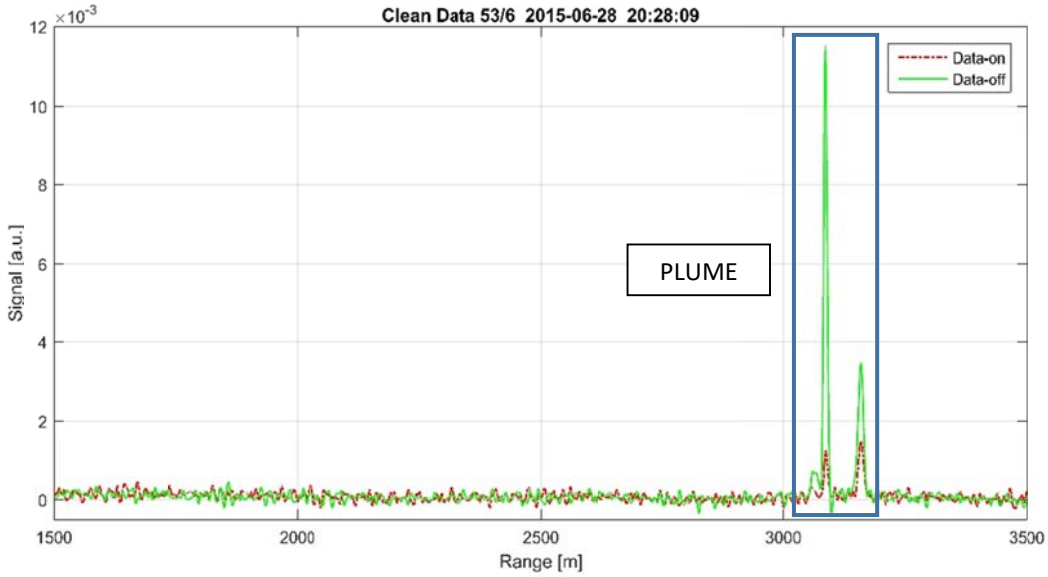

(B) 28/06/2015 – "Scansione Verticale 5" – Loop6/Signal61. El:18.1° - Az:237.8°

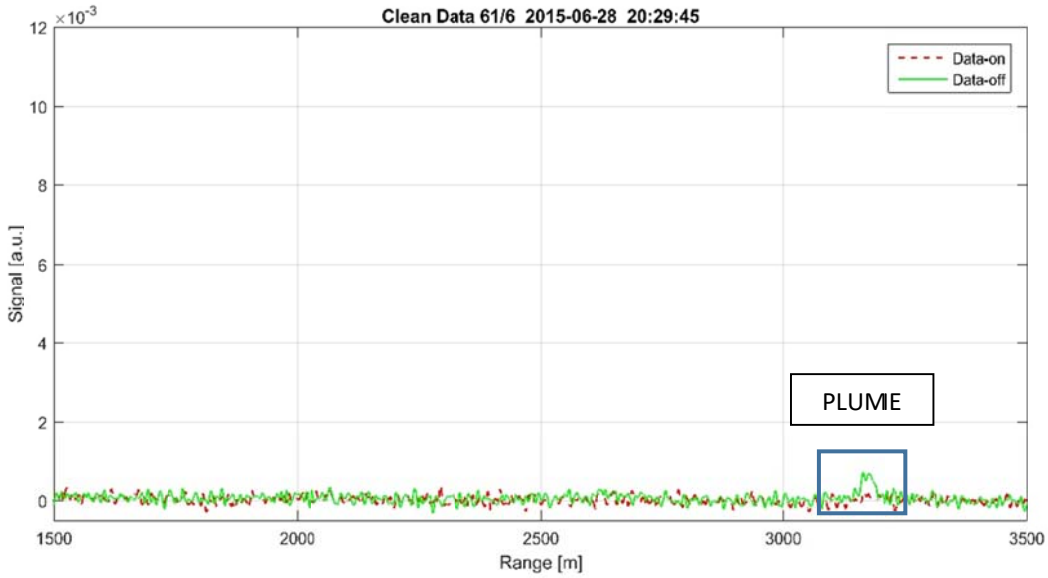

(C) 28/06/2015 – "Scansione Verticale 5" – Loop6

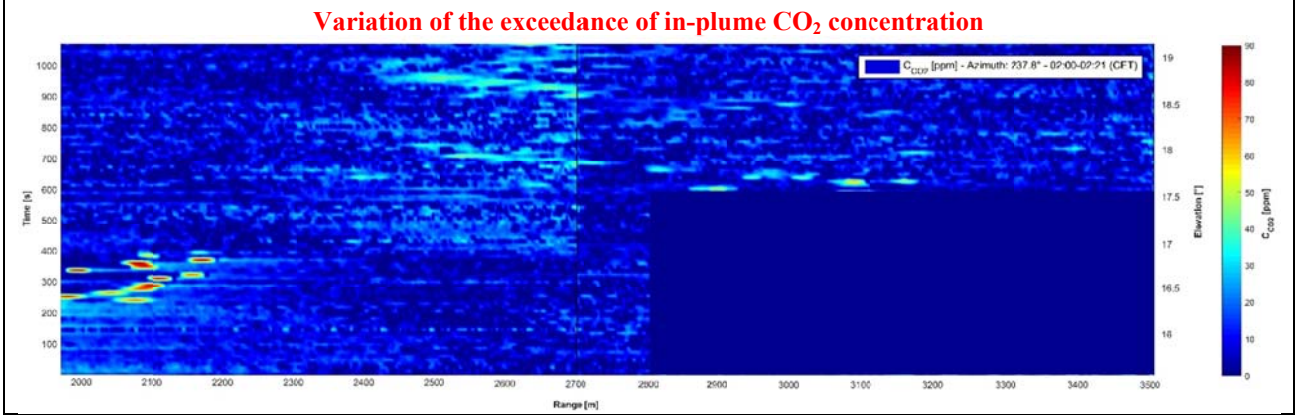

Figure 28) A – *Example of Lidar profile n°53, Loop6, "Scansione Verticale 5", Elevation angle: 17.78°, Azimuth angle: 237.8°. It is possible to see a triple CO_2 in-plume peak between 3 Km and 3.2 Km.* **B** – *Example of Lidar profile n°61, Loop6, "Scansione Verticale 5", Elevation angle: 18.1°, Azimuth angle: 237.8°. It is possible to see a CO_2 in-plume peak between 3.2 Km and 3.3 Km.* **C** *- Vertical scan in Cartesian coordinates of the exceedance of in-plume CO_2 concentration related to Loop1 of "Scansione Verticale 5" as a function of range [m], elevation angle [°] and time [s]. It is possible to see some traces of in-plume CO_2 concentration on the left, on the upper side of the Figure and beyond 3 Km, for elevation angles greater than the threshold of Vancori's peak. As already stressed in Figure 25, the high density of CO_2 plume traces could be probably due to the increase in relative humidity during the nighttime session. This phenomenon, combined with the effect of the wind, has probably scattered the plume traces from the side of Pizzo above the Vancori's peak and then up in the atmosphere.*
Note that the dark blue portion indicate an interval without measurements.
NB) LOS of the system was pointed to Vancori (rockface).

4.6 29/06/2015

During the measurement session of the 29 of June, 2015; a significant amount of in-plume CO_2 concentration traces have been detected in the following scan:

- "Scansione Verticale 5" – vertical scan, data acquired from 11:49 p.m. to 06:34 a.m. – Figure 29 (second part).

For further details about the main characteristics of this session, reference is made to Table 7.

"Scansione Verticale 5" (18-40 Loop)

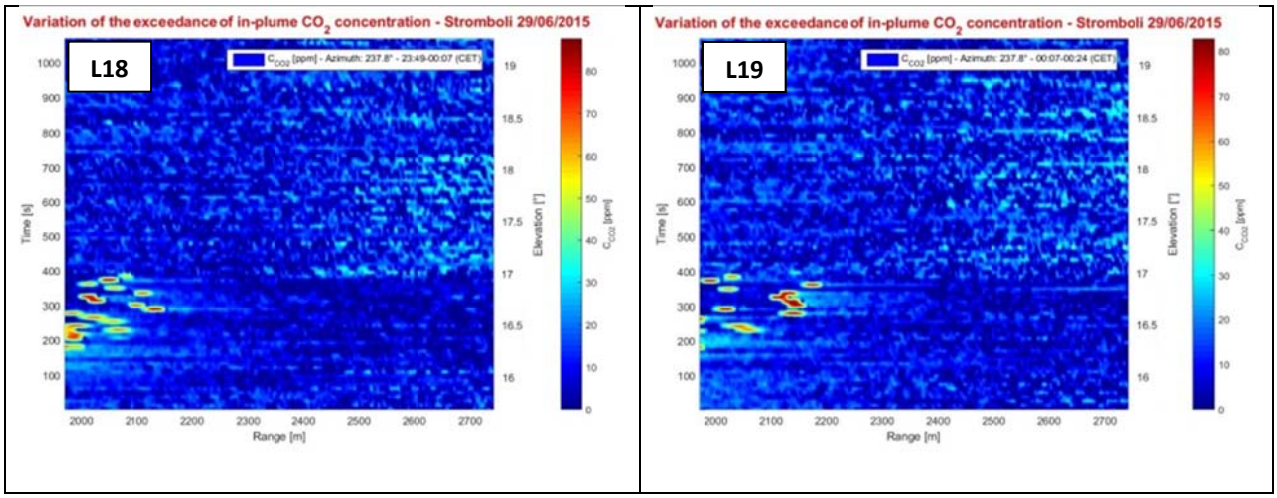

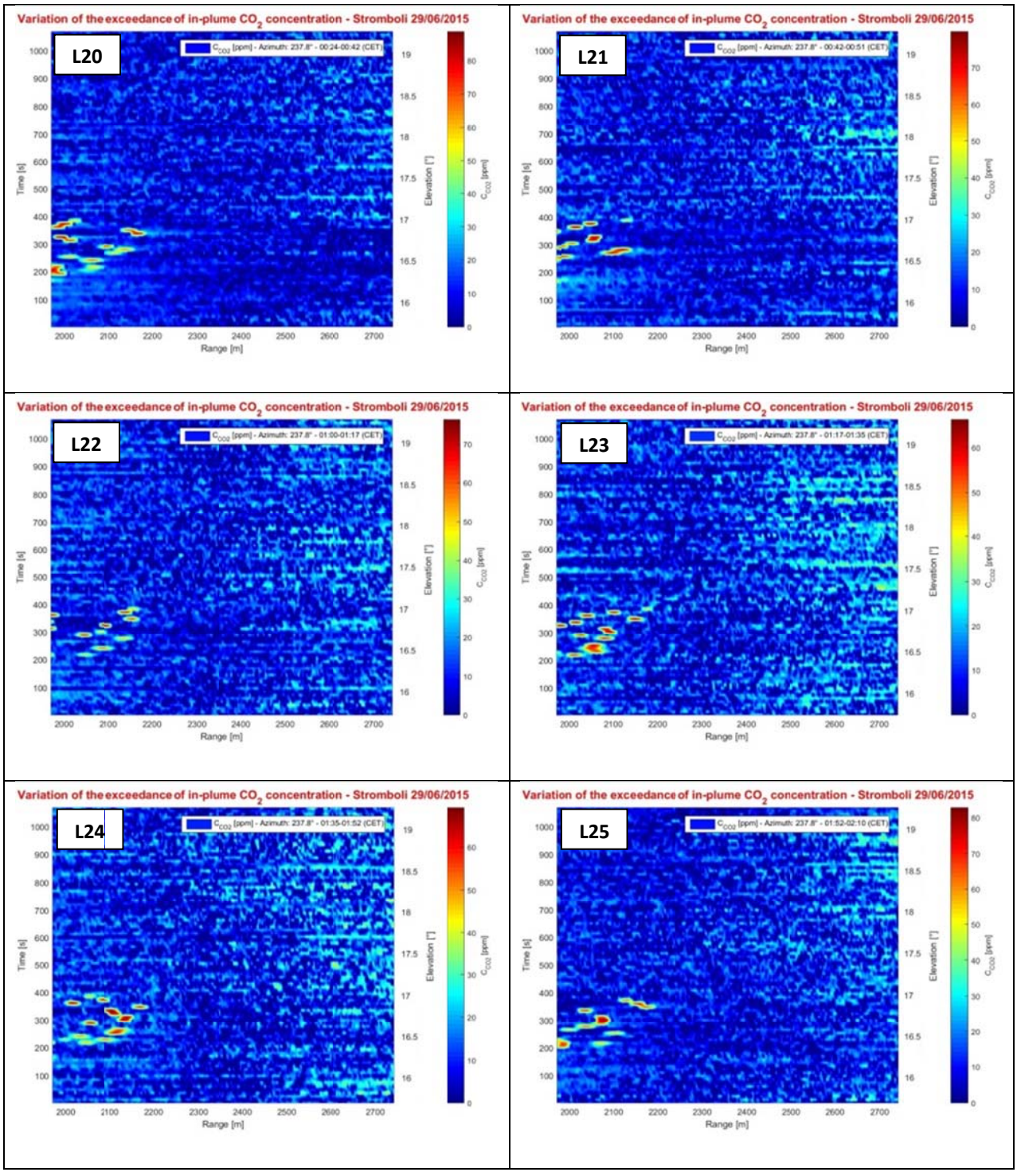
Variation of the exceedance of in-plume CO_2 concentration - Stromboli 29/06/2015
L20
C_{CO2} [ppm] - Azimuth: 237.8° - 00:24-00:42 (CET)
Time [s]
Range [m]
Elevation [°]
C_{CO2} [ppm]
Variation of the exceedance of in-plume CO_2 concentration - Stromboli 29/06/2015
L21
C_{CO2} [ppm] - Azimuth: 237.8° - 00:42-00:51 (CET)
Time [s]
Range [m]
Elevation [°]
C_{CO2} [ppm]
Variation of the exceedance of in-plume CO_2 concentration - Stromboli 29/06/2015
L22
C_{CO2} [ppm] - Azimuth: 237.8° - 01:00-01:17 (CET)
Time [s]
Range [m]
Elevation [°]
C_{CO2} [ppm]
Variation of the exceedance of in-plume CO_2 concentration - Stromboli 29/06/2015
L23
C_{CO2} [ppm] - Azimuth: 237.8° - 01:17-01:35 (CET)
Time [s]
Range [m]
Elevation [°]
C_{CO2} [ppm]
Variation of the exceedance of in-plume CO_2 concentration - Stromboli 29/06/2015
L24
C_{CO2} [ppm] - Azimuth: 237.8° - 01:35-01:52 (CET)
Time [s]
Range [m]
Elevation [°]
C_{CO2} [ppm]
Variation of the exceedance of in-plume CO_2 concentration - Stromboli 29/06/2015
L25
C_{CO2} [ppm] - Azimuth: 237.8° - 01:52-02:10 (CET)
Time [s]
Range [m]
Elevation [°]
C_{CO2} [ppm]

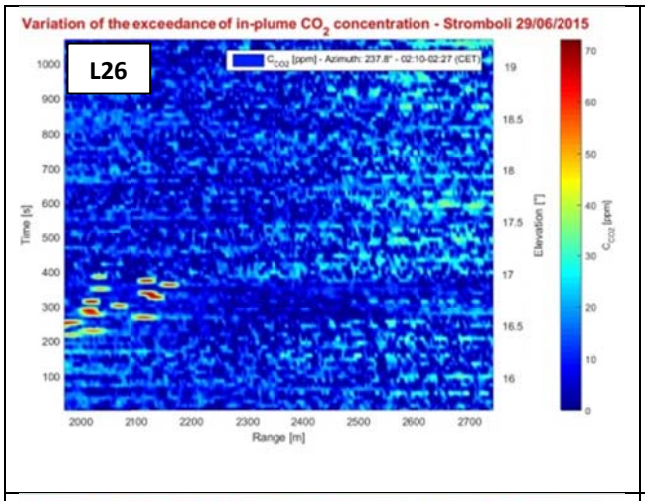
Variation of the exceedance of in-plume CO_2 concentration - Stromboli 29/06/2015
L26
C_{CO2} [ppm] - Azimuth: 237.8° - 02:10-02:27 (CET)
Time [s]
Range [m]
Elevation [°]
C_{CO2} [ppm]

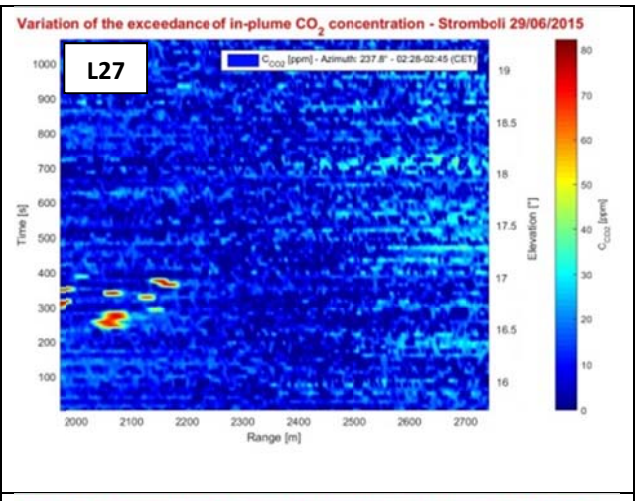
Variation of the exceedance of in-plume CO_2 concentration - Stromboli 29/06/2015
L27
C_{CO2} [ppm] - Azimuth: 237.8° - 02:28-02:45 (CET)
Time [s]
Range [m]
Elevation [°]
C_{CO2} [ppm]

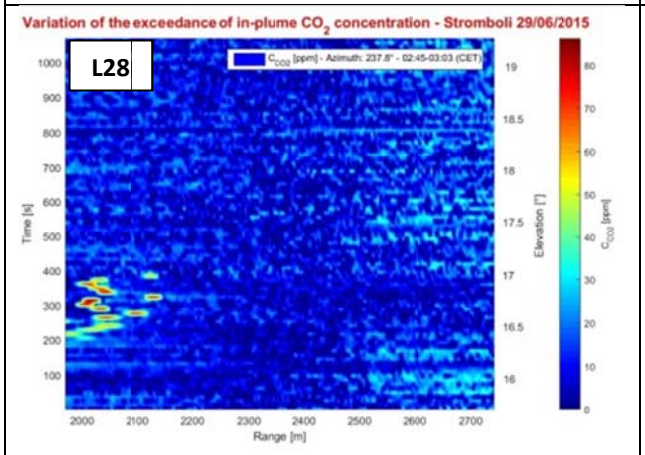
Variation of the exceedance of in-plume CO_2 concentration - Stromboli 29/06/2015
L28
C_{CO2} [ppm] - Azimuth: 237.8° - 02:45-03:03 (CET)
Time [s]
Range [m]
Elevation [°]
C_{CO2} [ppm]

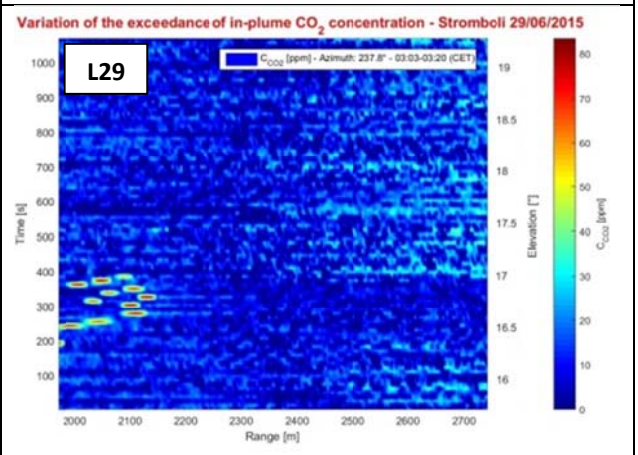
Variation of the exceedance of in-plume CO_2 concentration - Stromboli 29/06/2015
L29
C_{CO2} [ppm] - Azimuth: 237.8° - 03:03-03:20 (CET)
Time [s]
Range [m]
Elevation [°]
C_{CO2} [ppm]

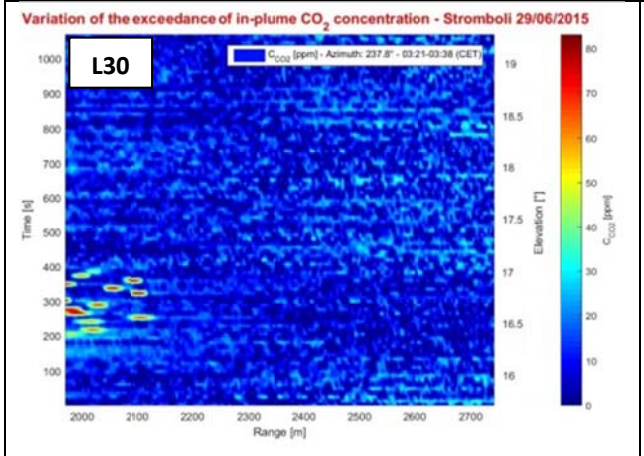
Variation of the exceedance of in-plume CO_2 concentration - Stromboli 29/06/2015
L30
C_{CO2} [ppm] - Azimuth: 237.8° - 03:21-03:38 (CET)
Time [s]
Range [m]
Elevation [°]
C_{CO2} [ppm]

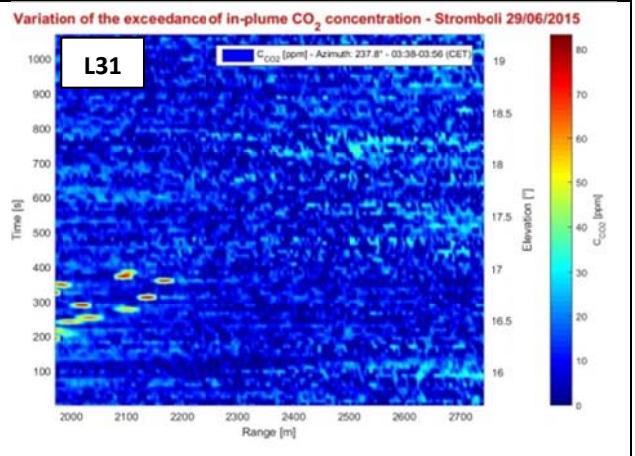
Variation of the exceedance of in-plume CO_2 concentration - Stromboli 29/06/2015
L31
C_{CO2} [ppm] - Azimuth: 237.8° - 03:38-03:56 (CET)
Time [s]
Range [m]
Elevation [°]
C_{CO2} [ppm]

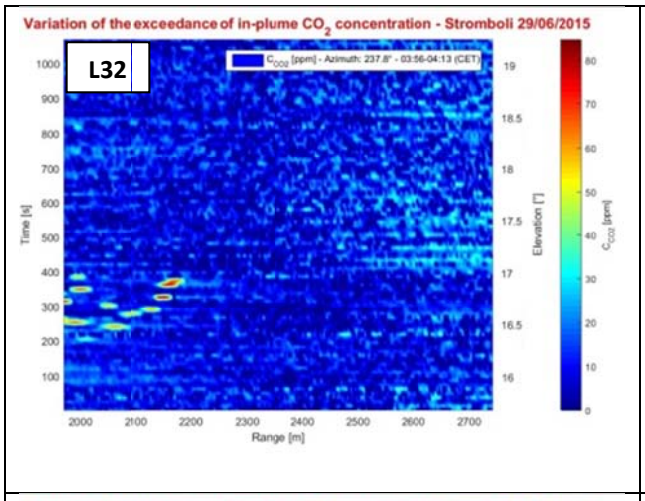
Variation of the exceedance of in-plume CO_2 concentration - Stromboli 29/06/2015
L32
C_{CO2} [ppm] - Azimuth: 237.8° - 03:56-04:13 (CET)
Time [s]
Range [m]
Elevation [°]
C_{CO2} [ppm]

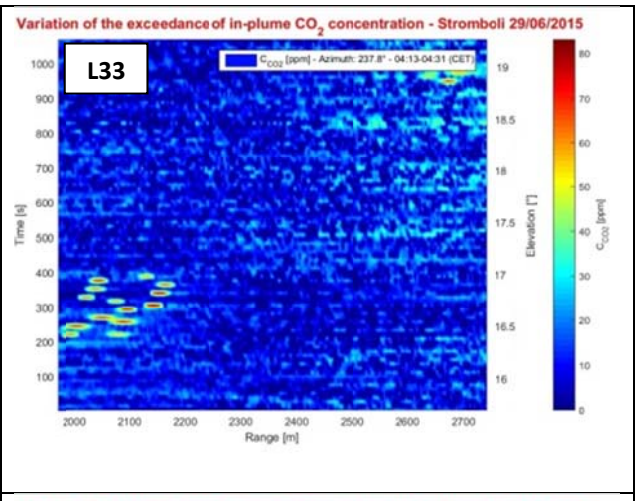
Variation of the exceedance of in-plume CO_2 concentration - Stromboli 29/06/2015
L33
C_{CO2} [ppm] - Azimuth: 237.8° - 04:13-04:31 (CET)
Time [s]
Range [m]
Elevation [°]
C_{CO2} [ppm]

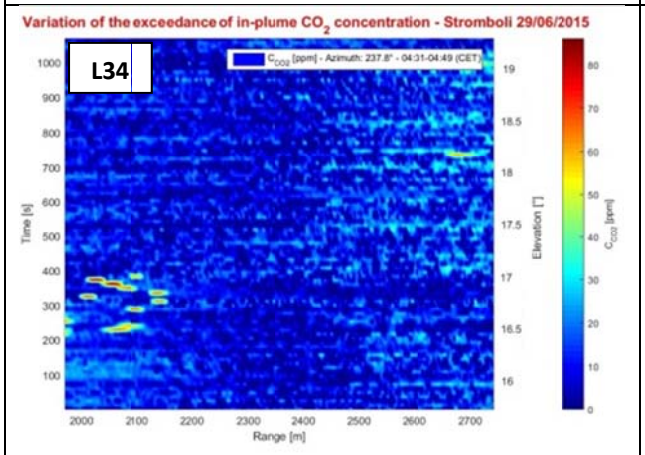
Variation of the exceedance of in-plume CO_2 concentration - Stromboli 29/06/2015
L34
C_{CO2} [ppm] - Azimuth: 237.8° - 04:31-04:49 (CET)
Time [s]
Range [m]
Elevation [°]
C_{CO2} [ppm]

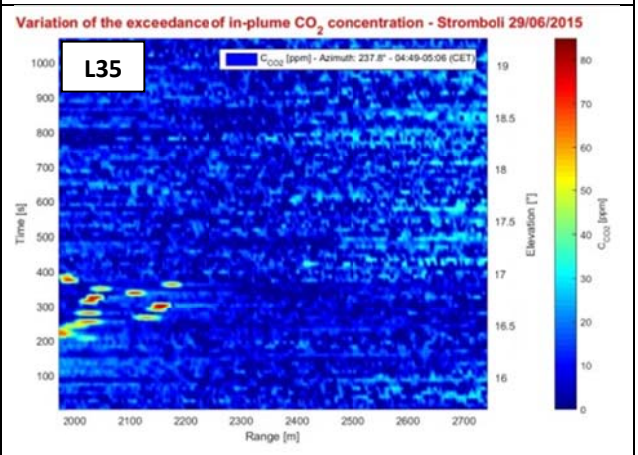
Variation of the exceedance of in-plume CO_2 concentration - Stromboli 29/06/2015
L35
C_{CO2} [ppm] - Azimuth: 237.8° - 04:49-05:06 (CET)
Time [s]
Range [m]
Elevation [°]
C_{CO2} [ppm]

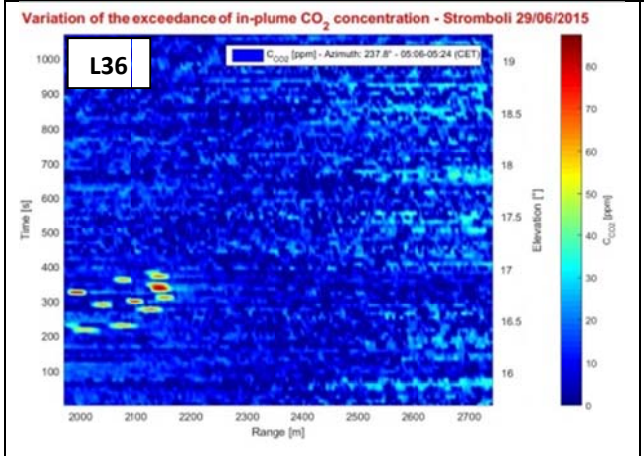
Variation of the exceedance of in-plume CO_2 concentration - Stromboli 29/06/2015
L36
C_{CO2} [ppm] - Azimuth: 237.8° - 05:06-05:24 (CET)
Time [s]
Range [m]
Elevation [°]
C_{CO2} [ppm]

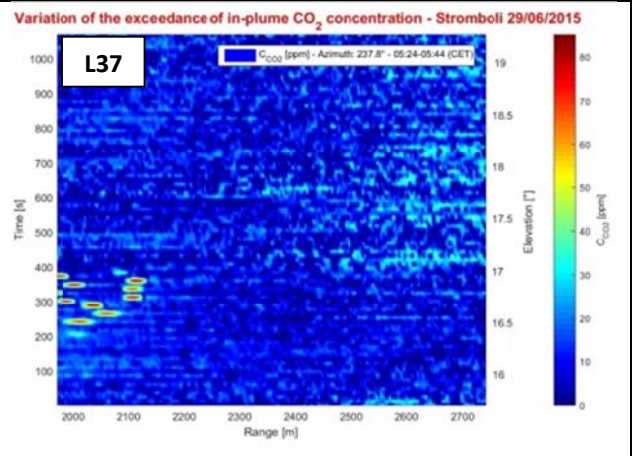
Variation of the exceedance of in-plume CO_2 concentration - Stromboli 29/06/2015
L37
C_{CO2} [ppm] - Azimuth: 237.8° - 05:24-05:44 (CET)
Time [s]
Range [m]
Elevation [°]
C_{CO2} [ppm]

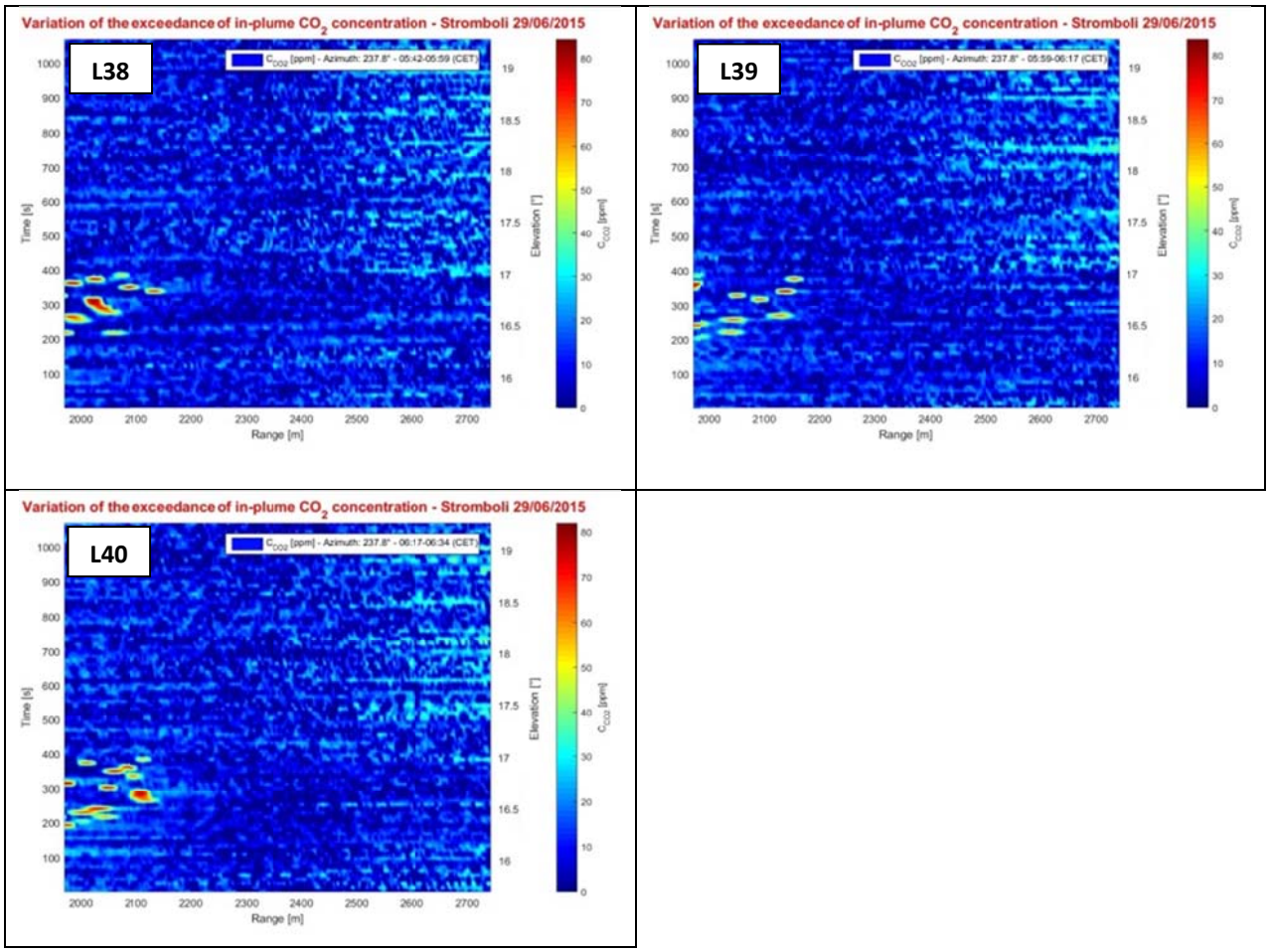

Figure 29) *The twentythree vertical loops (L8….L40) of the scan have been chronological rearranged so as to show the time evolution of the exceedance of in-plume CO_2 concentration. In the bottom left corner of each scan (in Cartesian coordinates) it is possible to see the variations of CO_2 concentration as a function of time and elevation. It is important to note that plume traces in the bottom left corner are extremely dense and continuously change their position; instead plume traces on the upper right side are less dense but more spread than the previous ones. As already shown in Figures 18, 24 and 27 this fact is particularly true during the nighttime session and could be probably due to the increase in relative humidity (therefore, CO_2 molecules have been condensed into the atmosphere and their scattering properties have been increased), combined with the effect of the wind that have scattered the plume traces above the rockface of Pizzo. NB) LOS of the system was pointed to Vancori (rockface).*

5. Conclusions

In this work, the results of the experimental campaign carried out between the 24 and the 29 of June, 2015, at Stromboli Volcano island have been reported. The main goal was to detect and analyze volcanic plumes, in order to measure the exceedance of in-plume CO_2 (the most reliable gas precursor to an eruption) concentration, for early warning of volcanic eruptions. For this purpose, BILLI, a differential absorption lidar for three-dimensional profiling of carbon dioxide in volcanic plumes, has been developed at the Frascati Research Center of ENEA under the ERC BRIDGE project.

A brief description of BILLI system and the newly designed BRIDGE DIAL technique has been done, respectively, in chapter 1 and 2. Moreover, an overview about the experimental set-up of the system and the meteorological conditions during the measurement sessions has been done in chapter 3. Finally, a fully comprehensive analysis of the field operations and, in particular, of CO_2 profiles and dispersion maps, achieved by Matlab routines, has been discussed in chapter 4.

The great novelty/advantage of the measurements reported here is that BILLI allowed measurements to be taken continuously, remotely (more than 3 Km) and, therefore, from a safer location free from risks to which operators are exposed during direct sampling, with much higher temporal (10 s) and spatial (1.5 m) resolution (the plume was scanned in few minutes rather than over several hours). These performances are adequate to follow the spatiotemporal dynamics of the volcanic plume and can provide, quickly and continuously, reliable data on a key precursor of volcanic eruptions.

In conclusion, the BILLI DIAL system was used to retrieve three-dimensional tomographies of volcanic plumes at Stromboli Volcano. CO_2 excess of a few tens of ppm has been clearly detected remotely and in a few minutes scan. Furthermore, a complete time-resolved plume evolution has been detected in several measurement sessions, this fact could also be useful for the measurement of wind speed.

The lidar measurements were in good agreement with results obtained with conventional techniques, yet based on completely independent and significantly different approaches. This has proven the goodness and the reliability of the system developed at ENEA.

To our knowledge, this is the first time that carbon dioxide is retrieved by lidar in a volcanic plume, representing the first direct real-time measurement of this kind ever performed on an active volcano, overall demonstrating the high potential of laser remote sensing in volcanological research. In the near future, laser remote sensing systems could be important components of sensor networks dedicated to warn in advance the civilian population to natural hazards implied by active volcanos.

Acknowledgements

The authors are grateful to ENEA, in general, and Aldo Pizzuto, Roberta Fantoni and Antonio Palucci, in particular, for constant encouragement. They warmly thank Maria Sarcì, Dario Sisia and Raimondo Spadaro of ENEL for hosting BILLI inside the fence of the power plant and for electrical power. The support from the ERC project BRIDGE, n. 305377 is gratefully acknowledged.

References

[1] Aiuppa A, Fiorani L, Santoro S, Parracino S, Nuvoli M, Chiodini G, Minopoli C, Tamburello G (2015) New ground-based lidar enables volcanic CO2 flux measurements. Sci Rep 5: paper 13614, 12 pp

[2] Fiorani L, Santoro S, Parracino S, Maio I, Del Franco M and Aiuppa A (2015) LIDAR detection of carbon dioxide in volcanic plumes. Third International Conference on Remote Sensing and Geoinformation of the Environment (RSCy2015), Cyprus, June 19, 2015, Proc. SPIE 9535, doi:10.1117/12.2192724; http://dx.doi.org/10.1117/12.2192724.

[3] Fiorani L, Santoro S, Parracino S, Nuvoli M, Minopoli C and Aiuppa A (2015) Volcanic CO2 detection with a DFM/OPA-based lidar. Optics Letters March 2015; 40(6). doi:10.1364/OL.40.001034.

[4] Fiorani L, Saleh WR, Burton M, Puiu A, Queißer M (2013) Spectroscopic considerations on DIAL measurement of carbon dioxide in volcanic emissions. J Optoelectron Adv M 15: 317-325

[5] Hitran on the web - http://hitran.iao.ru/

[6] Fiorani L (2010) Lidar application to litosphere, hydrosphere and atmosphere. In: Koslovskiy VV (ed) Progress in Laser and Electro-Optics Research, Nova, New York, US, pp 21-75

[7] Rothman LS, Gordon IE, Barbe A, Benner DC, Bernath PF, Birk M, Boudon V, Brown LR, Campargue A, Champion J-P, Chance K, Coudert LH, Dana V, Devi VM, Fally S, Flaud J-M, Gamache RR, Goldman A, Jacquemart D, Kleiner I, Lacome N, Lafferty WJ, Mandin J-Y, Massie ST, Mikhailenko SN, Miller CE, Moazzen-Ahmadi N, Naumenko OV, Nikitin AV, Orphal J, Perevalov VI, Perrin A, Predoi-Cross A, Rinsland CP, Rotger M, Šimečková M, Smith MAH, Sung K, Tashkun SA, Tennyson J, Toth RA, Vandaele AC, VanderAuwera J (2009) The HITRAN 2008 molecular spectroscopic database. J Quant Spectrosc Radiat Transfer 110: 533-572

[8] Google Earth - https://www.google.it/intl/it/earth/

[9] MeteoBlue - https://www.meteoblue.com/it/tempo/previsioni/settimana/stromboli

[10] MeteoAM - http://www.meteoam.it/

ENEA
Servizio Promozione e Comunicazione
www.enea.it

Stampa: Laboratorio Tecnografico ENEA - C.R. Frascati
ottobre 2016